A New LMC PNLF and Kinematic Mapping Using PNe as Evolutionary Tracers

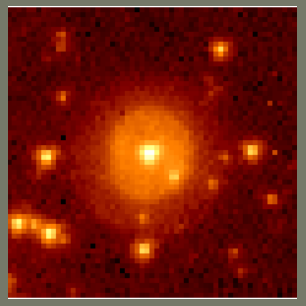

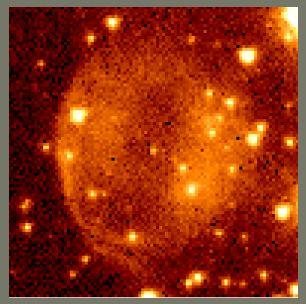

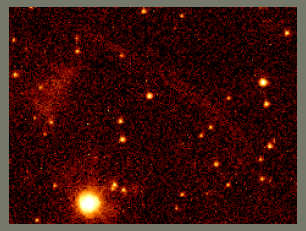

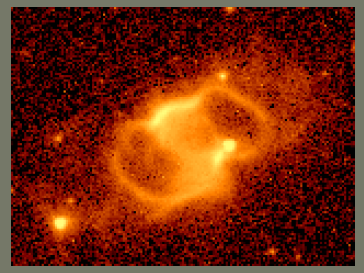

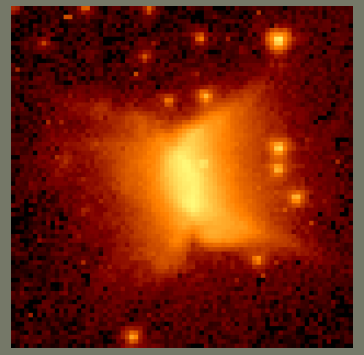

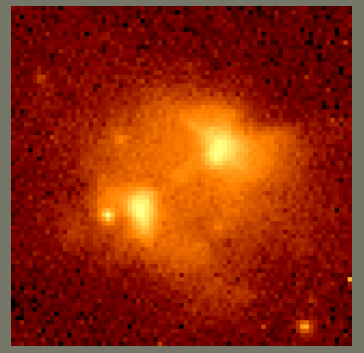

Warren Reid
Macquarie University, Australian Astronomical Observatory
Sydney, Australia

ESO Workshop on Deaths of Stars and Lives of Galaxies
Santiago de Chile
11 April, 2013

Australian Government
Department of Innovation Industry, Science and Research

AAO

MACQUARIE UNIVERSITY
ASTRONOMY, ASTROPHYSICS AND ASTROPHOTONICS RESEARCH CENTRE

MACQUARIE UNIVERSITY
SYDNEY ~ AUSTRALIA

Images and Spectra of New PNe

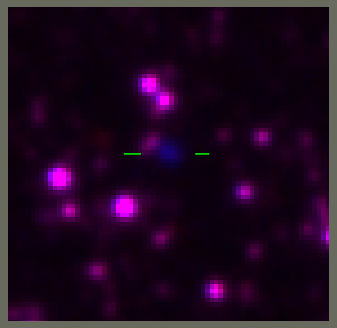

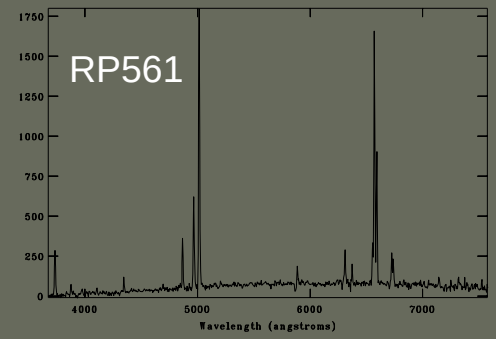

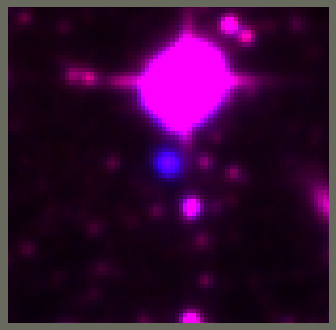

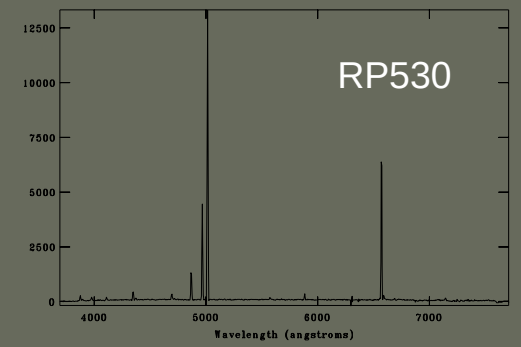

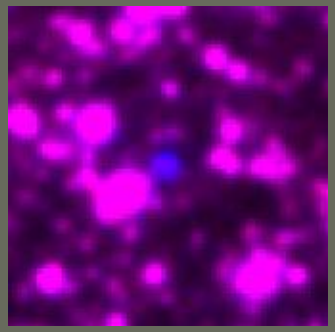

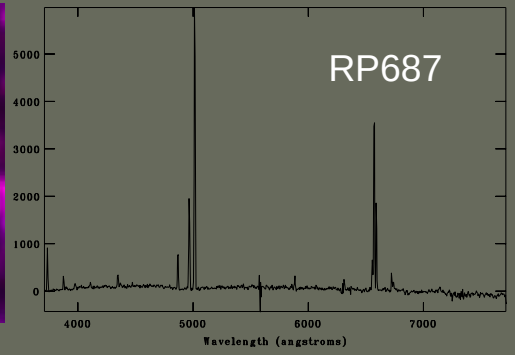

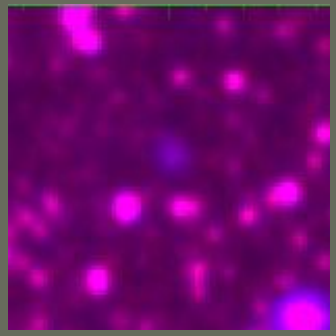

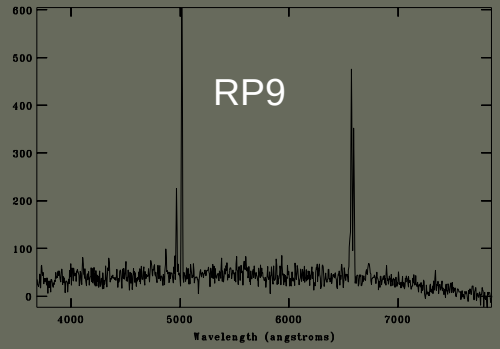

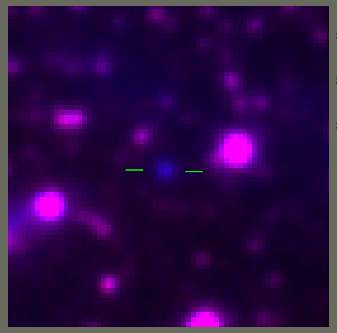

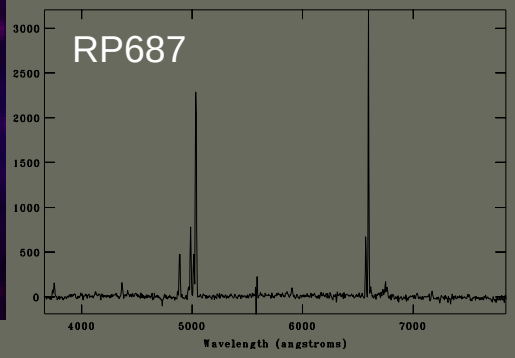

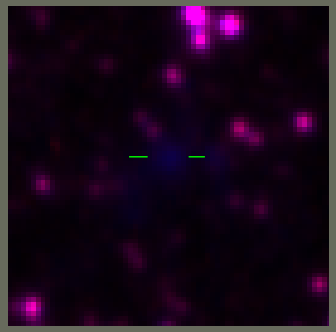

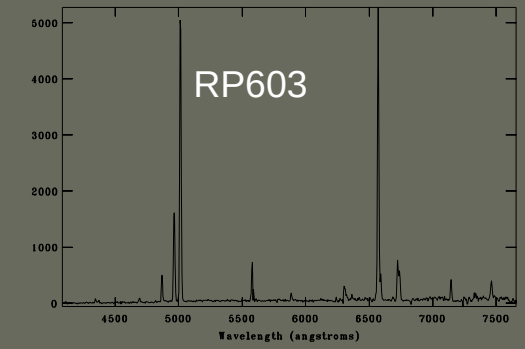

Images and Spectra of New PNe

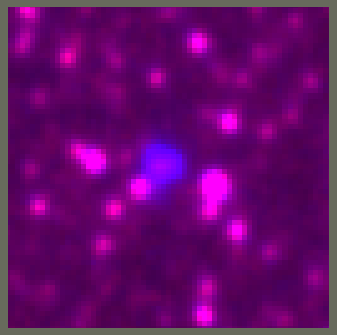

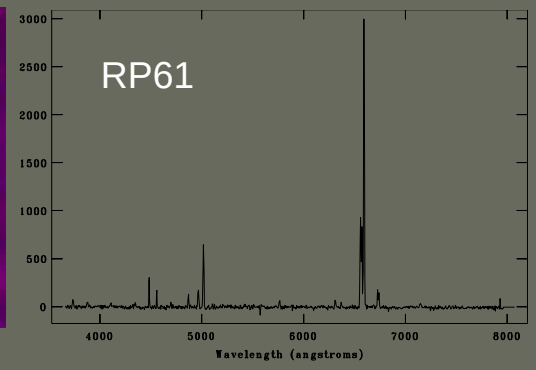

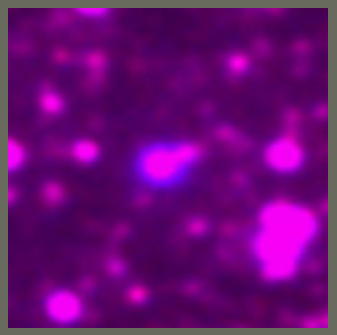

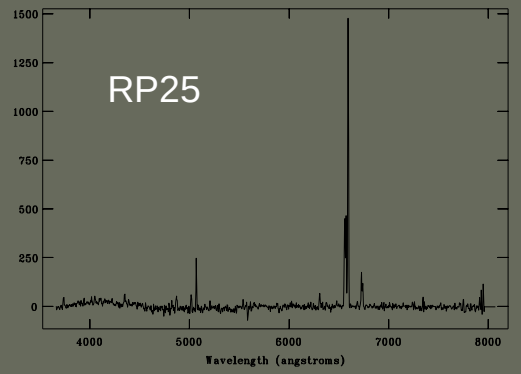

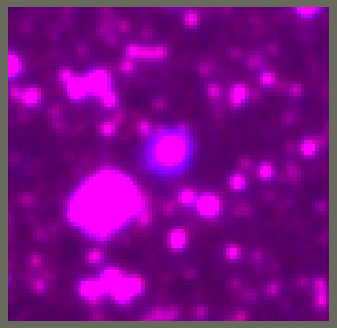

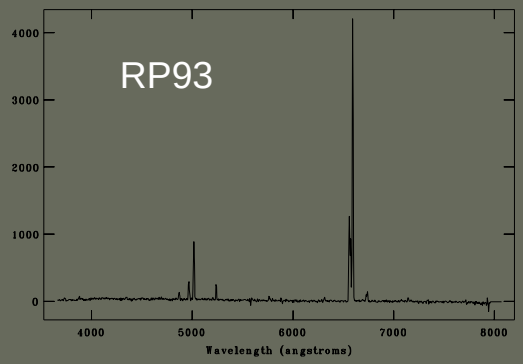

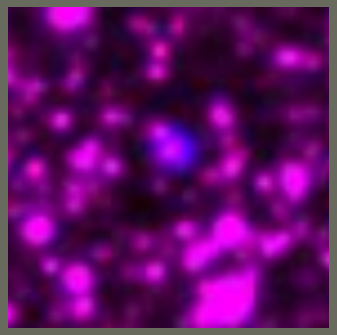

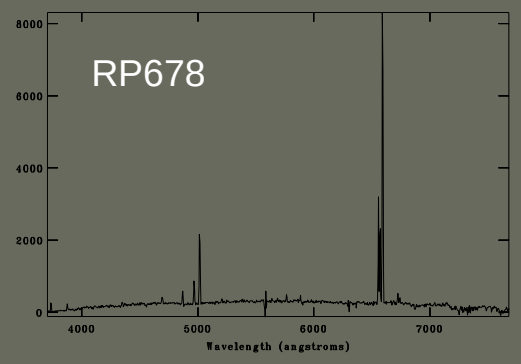

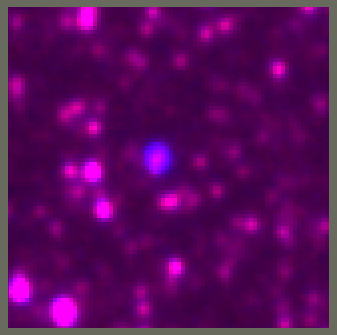

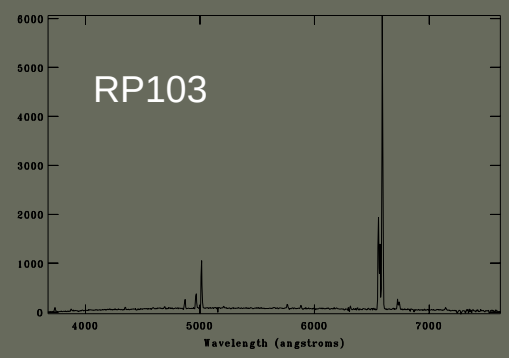

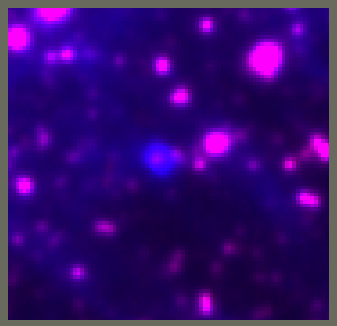

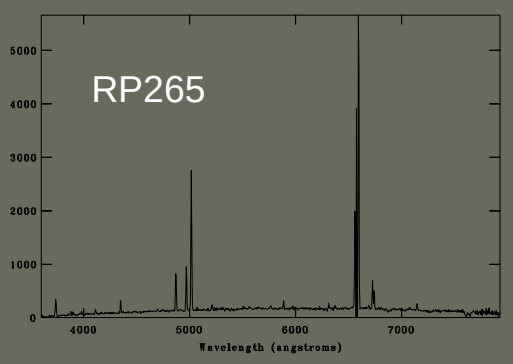

100% Candidate spectroscopic follow-up

Telescopes used :	Number of objects observed
2dF on the Anglo Australian Telescope	2,224*
1.9m at South African Astronomical Observatory	79
FLAMES multi-fibre spectrograph on the VLT	1260
Gemini South	18
MSSSO 2.3-m telescope	76
6dF on the UKST	573
AAOmega on the Anglo Australian Telescope	1,957

* This includes 3,683 low resolution (300B) and 3,838 medium resolution (1200R) spectra

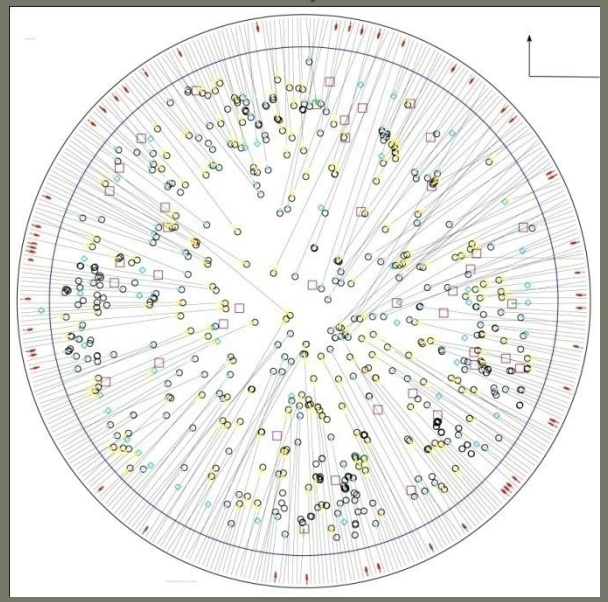

A 2dF field configuration

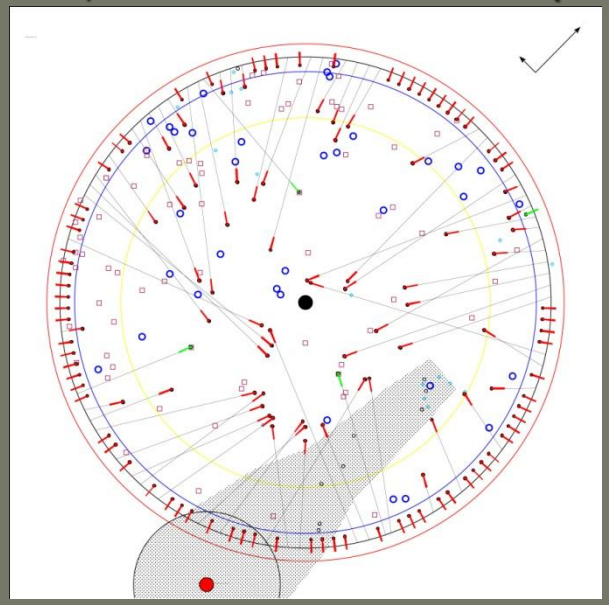

A VLT FLAMES field configuration

LMC PNe in the IR

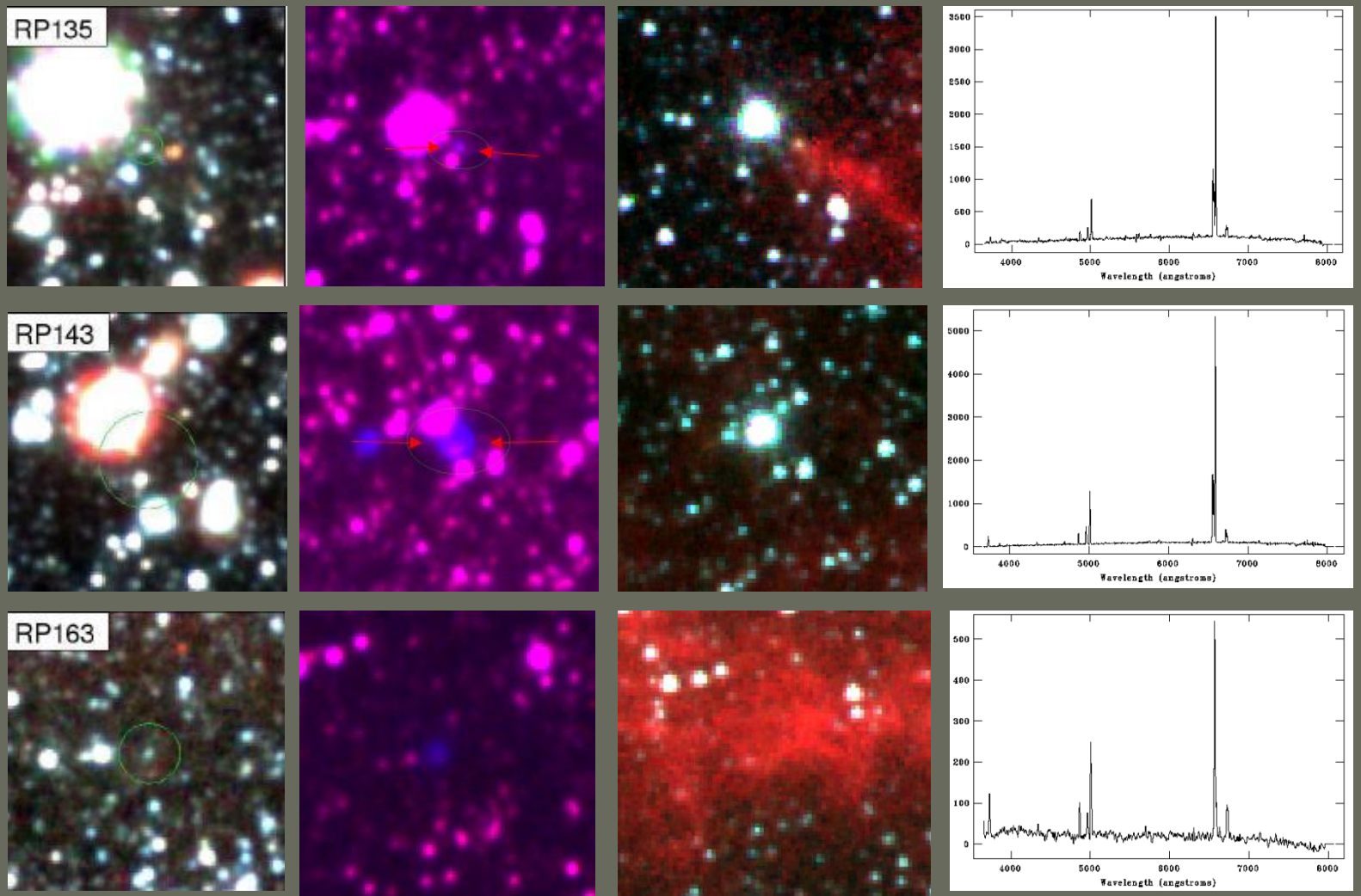

VMC K_s=R, J=G, Y=B

UKST Hα/R

SAGE IRAC R=5.8, G=4.5, B=3.6

Miszalski et al. 2011

LMC PNe in the IR

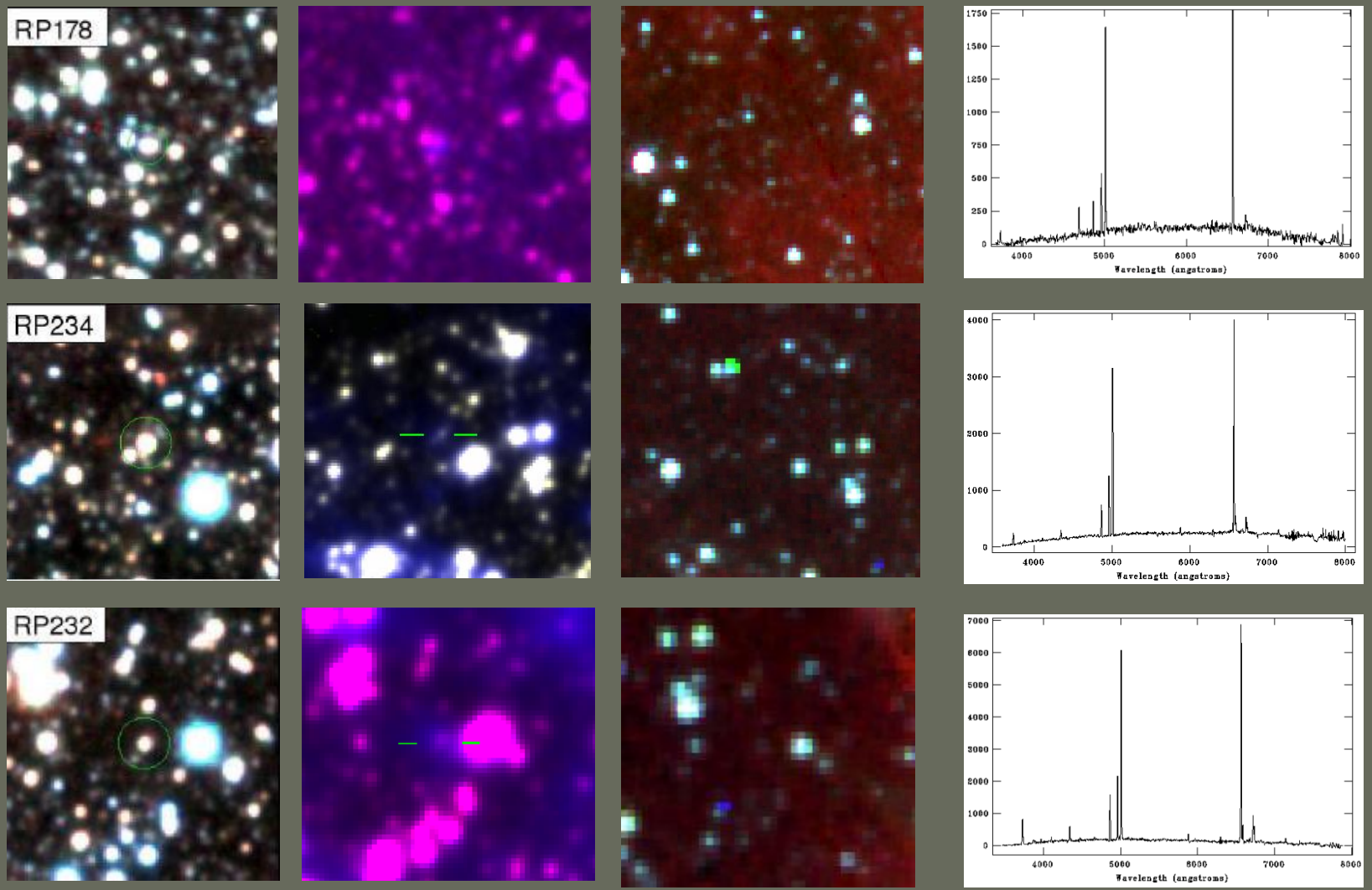

VMC K_s=R, J=G, Y=B

UKST Hα/R

SAGE R=5.8, G=4.5, B=3.6

Miszalski et al. 2011

HST Confirmation of RP PNe

Shaw, Reid, Parker, 2007 PASA 119, 19

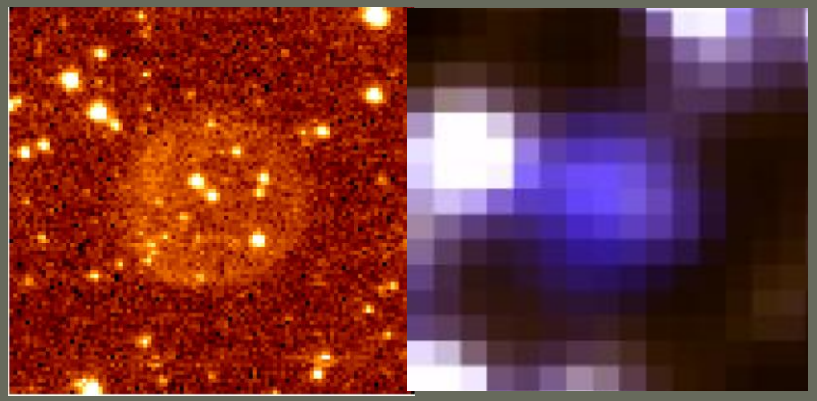

RP671

Left: HST image taken with WFPC2/F656N,
Right: UKST discovery image

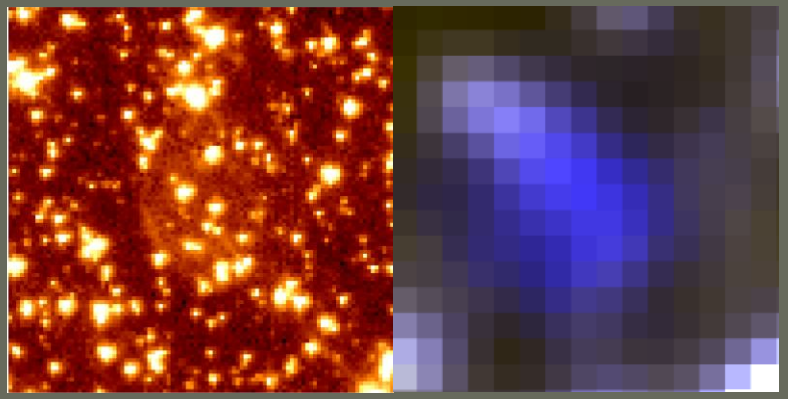

RP723

Above: HST image taken with WFPC2/F555W,
Right: UKST discovery image

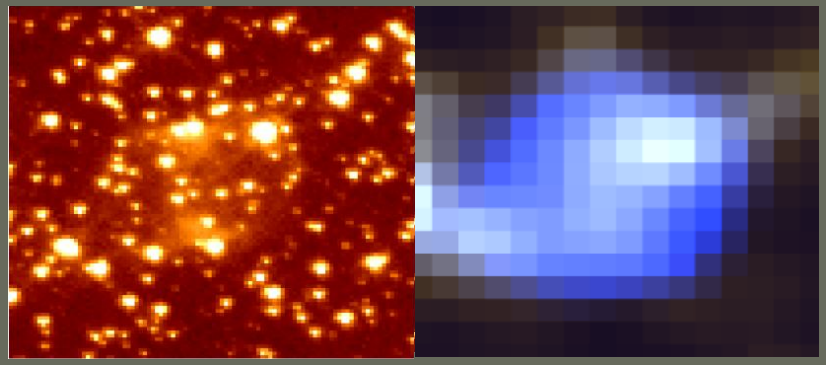

RP764

Left: HST image taken with WFPC2/F606W,
Right: UKST discovery image

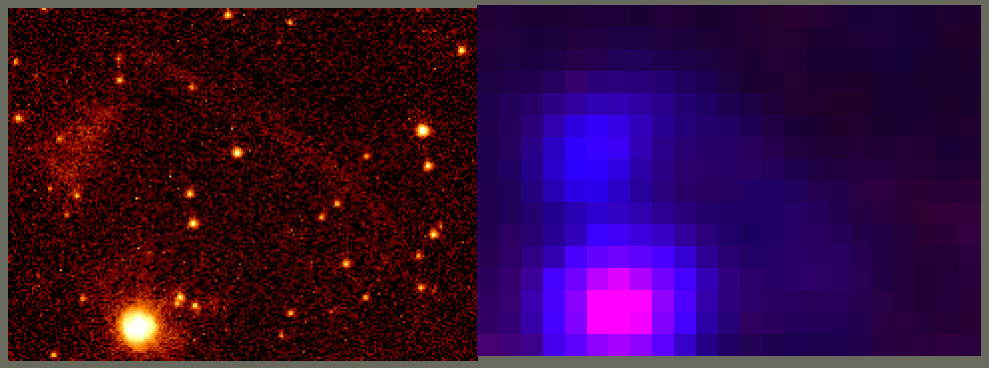

SMP 27

Left: HST broad band 9” x 12” image revealing faint outer structure
Right: UKST image covering the same area.

The next step

- This work has now been extended to the outer regions of the LMC through access to the MCELS data and the SuperCOSMOS Hα/R images. Several thousand additional compact emission candidates have been found. Subsequent follow-up spectroscopy on the 2dF AAOmega system on the AAT and 6dF on the UKST has so far led to a further 100 new faint PNe being discovered within the 56 deg^2 of the outer LMC. Again all previously known PNe were independently recovered.

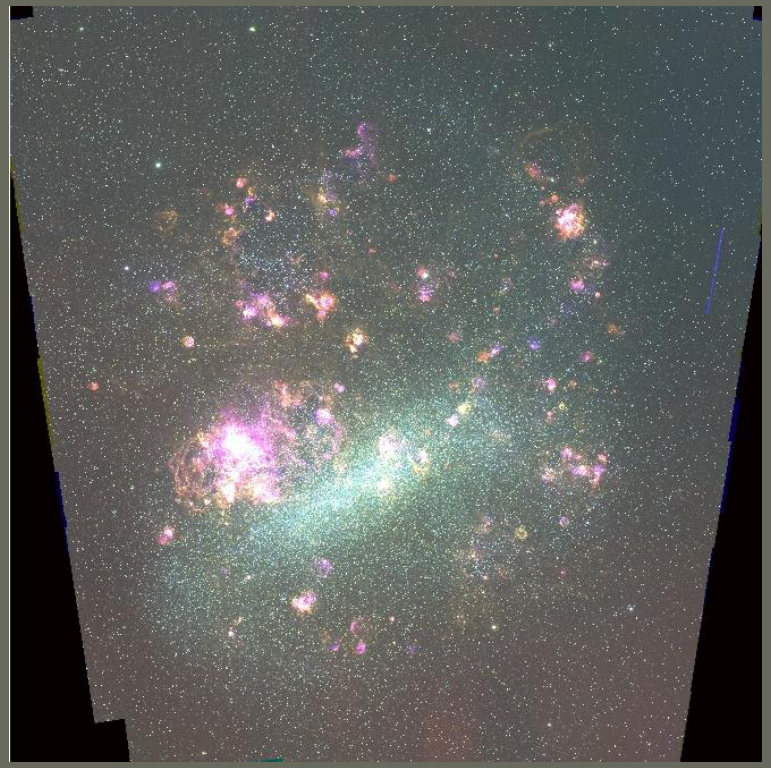

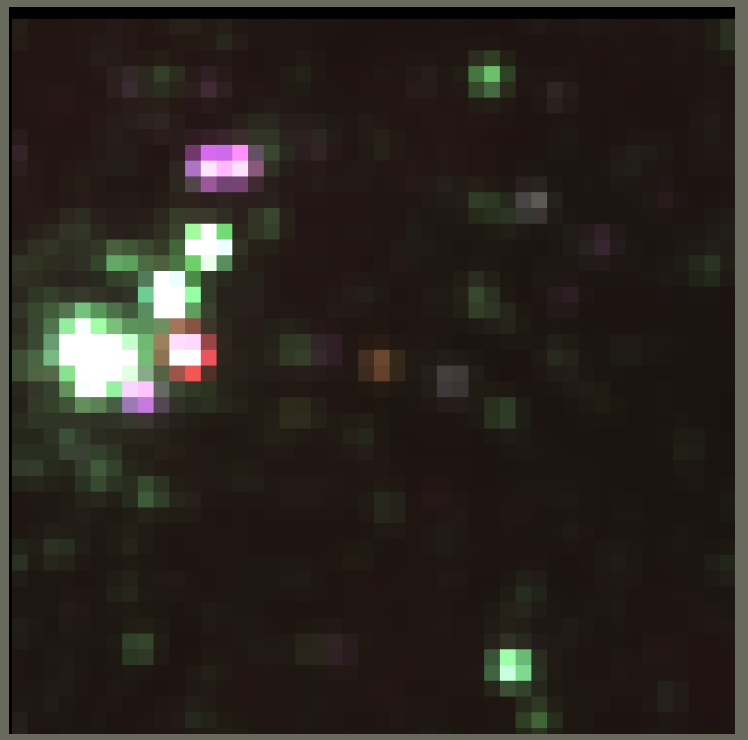

New and previously known PN uncovered through MCELS

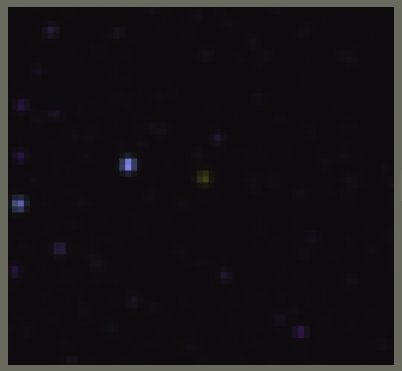

RP2271

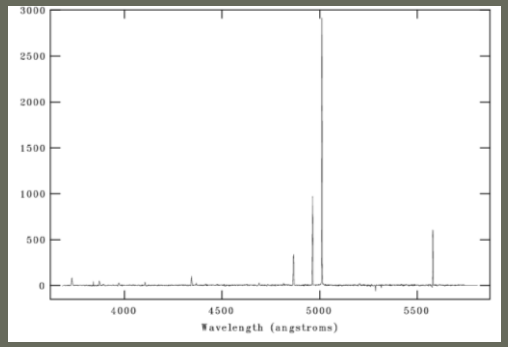

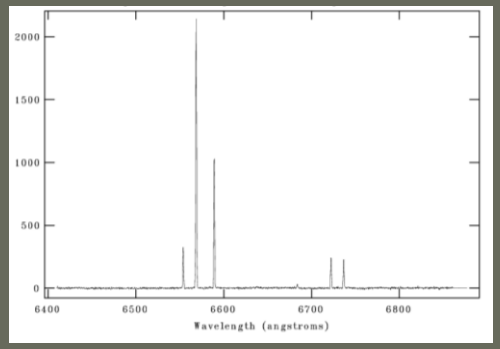

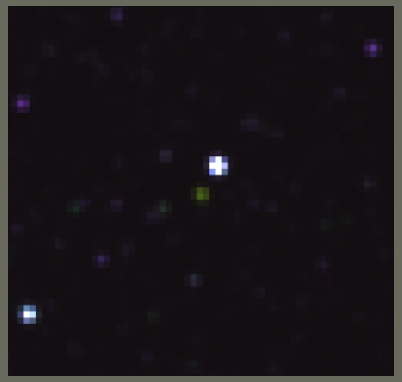

RP2294

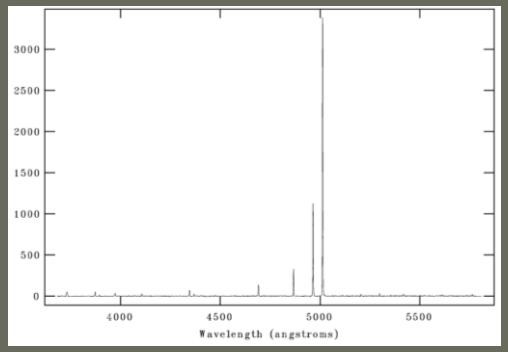

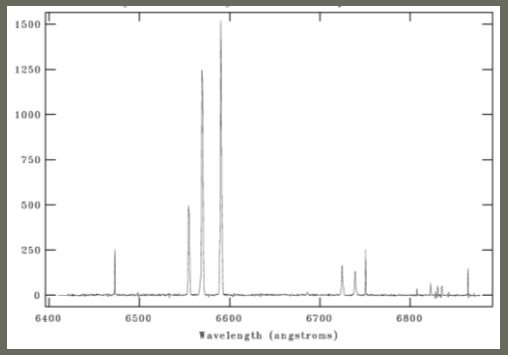

RP2314

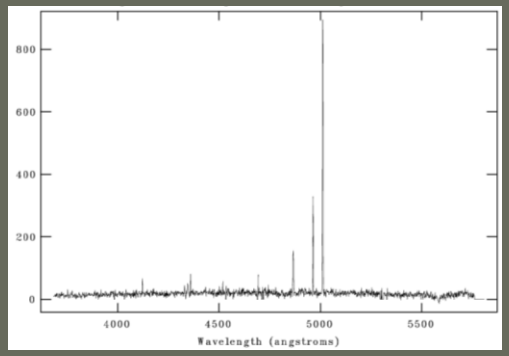

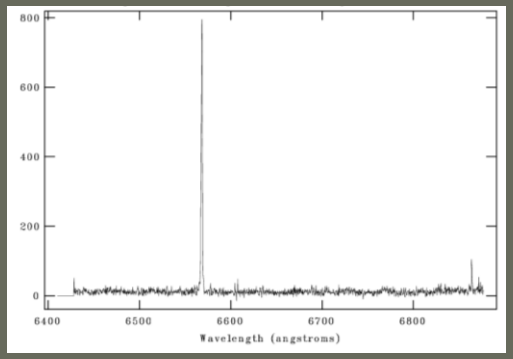

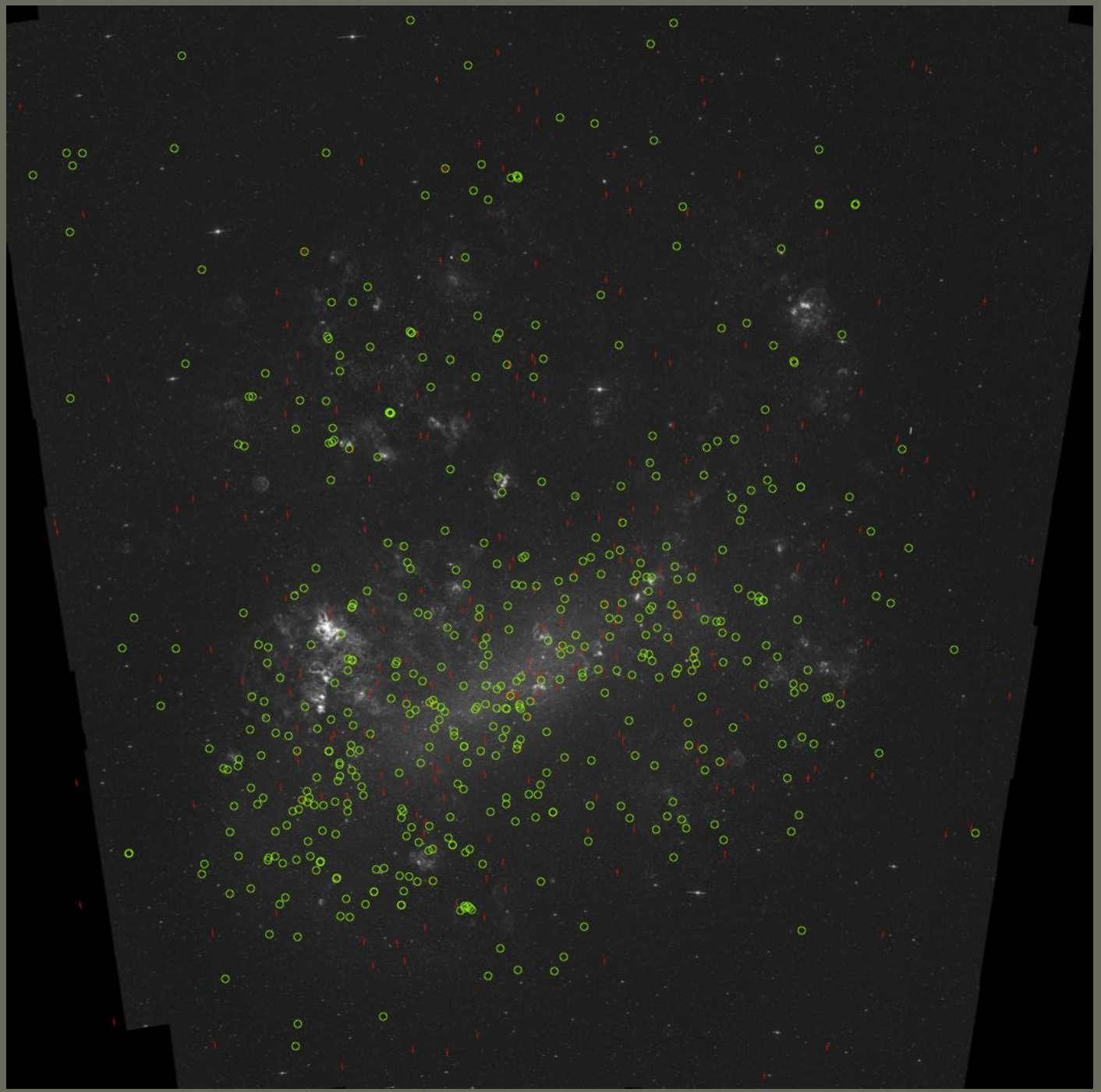

Spectral Diagnostics

Extinction

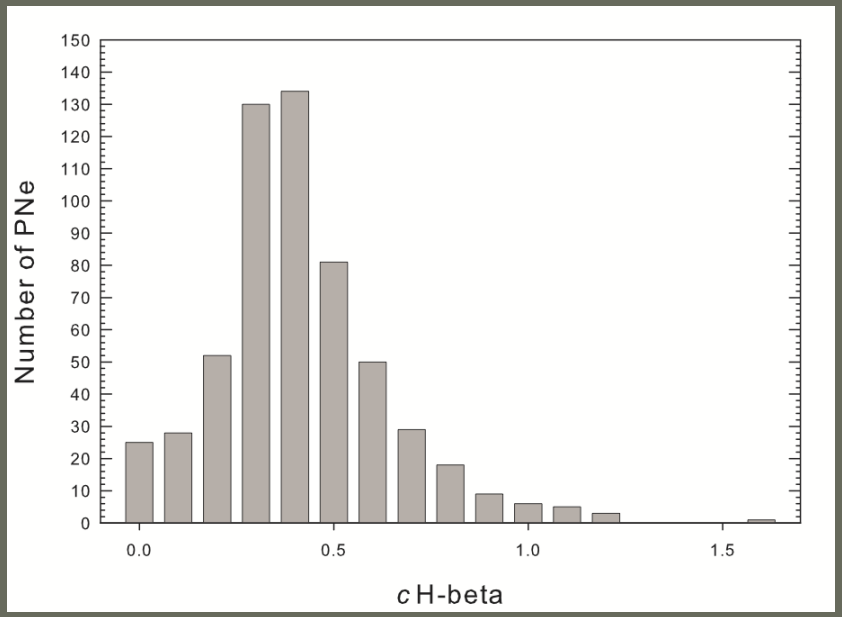

This estimation is based on the relationship between observed and intrinsic intensities:

$$\frac{I_{obs}(H\alpha)}{I_{obs}(H\beta)} = \frac{I_{int}(H\alpha)}{I_{int}(H\beta)} \; 10^{-c(H\beta)[f(H\alpha)-f(H\beta)]}$$

All other lines were corrected for reddening using:

$$\frac{I_{cor}(\lambda)}{I_{cor}(H\beta)} = \frac{I_{obs}(\lambda)}{I_{obs}(H\beta)} \; 10^{cf(\lambda)}$$

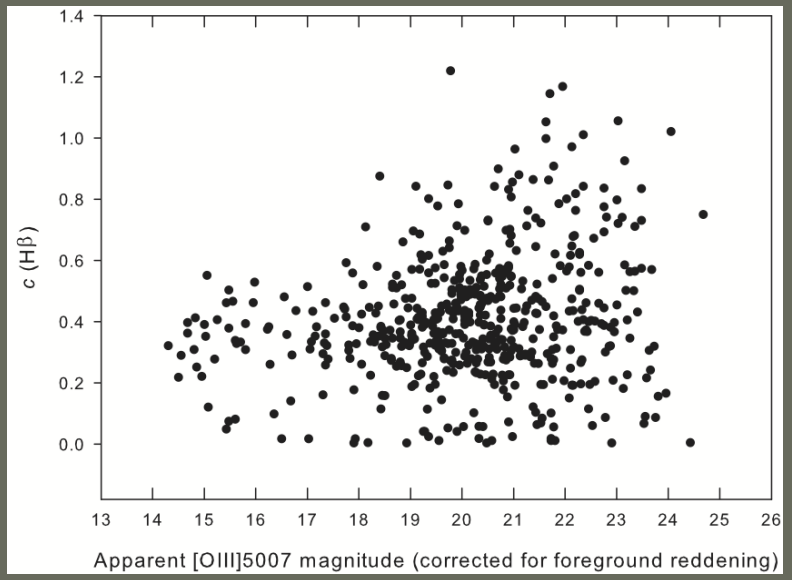

A peak at 0.6 shows the low overall extinction of most LMC PNe. Most of the bright PNe occupy the range 0.1-0.6.

$$c(H\beta) = 2.875 \; log\,(H\alpha/H\beta) / 2.85$$

Planetary Nebula Luminosity Function

2010 MNRAS 405, 1349

A New Population of Planetary Nebulae Discovered in the Large Magellanic Cloud (III): The Luminosity Function

Warren A. Reid[1]* and Quentin A. Parker [1,2]†
[1]Department of Physics, Macquarie University, Sydney, NSW 2109, Australia
[2]Anglo-Australian Observatory, PO Box 296, Epping, NSW 1710 Australia

Corrected for foreground extinction in order to make a direct comparison to previous PNLFs from other galaxies where internal dust extinction is unable to be derived.
E(B-V) = 0.074 for the LMC. Av_{5007} = 0.1074 mag

Now extends over 10+ magnitude range- faint end shape elucidated

Rapid rise from mag 18 at the bright end not observed previously but was predicted due to the mean age of 3-8 Gyr for stars in the LMC (Stryker & Butcher 1981; Frogel & Blanco 1983; Hyland 1991)

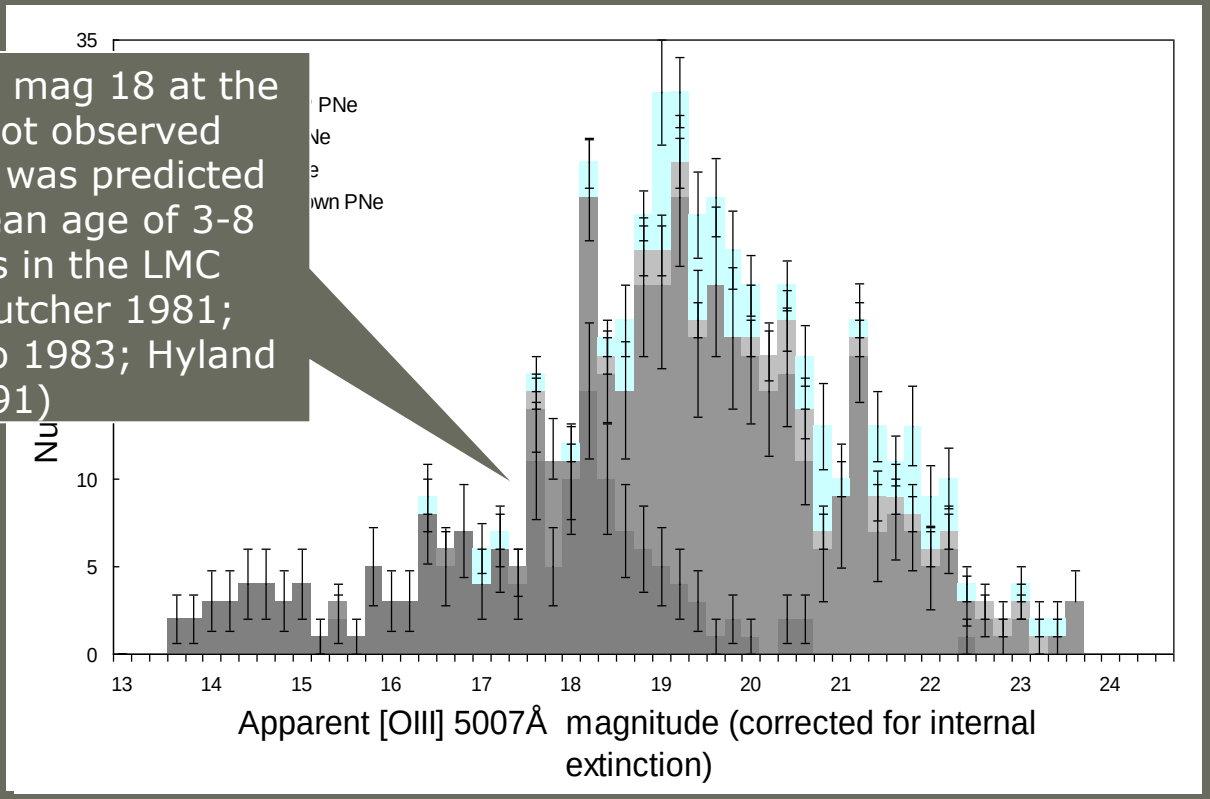

Planetary Nebula Luminosity Function

PNLF as a distance indicator

2010 MNRAS 405, 1349

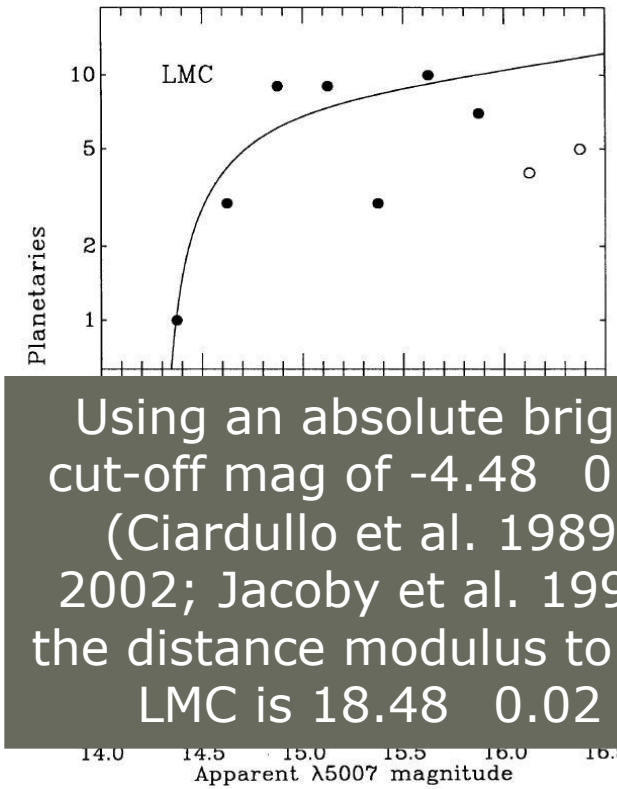

Using an absolute bright cut-off mag of -4.48 0.05 (Ciardullo et al. 1989, 2002; Jacoby et al. 1992) the distance modulus to the LMC is 18.48 0.02

PNLF from Jacoby, Walker, Ciardullo, 1990, ApJ 365, 471

$$N(M) \propto e^{0.307M}\{1 - e^{3(M^* - M)}\}$$

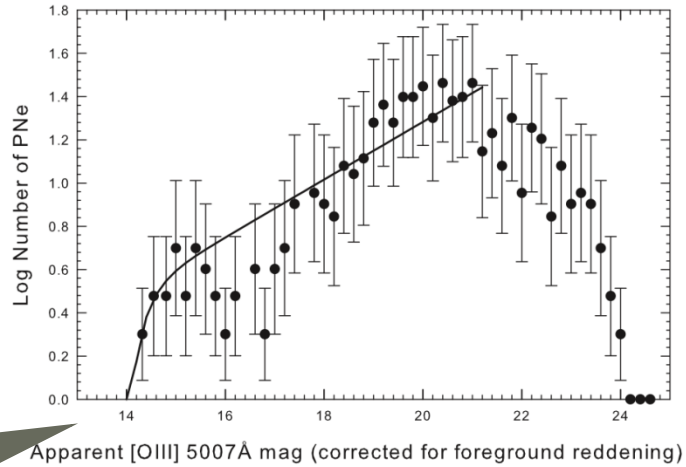

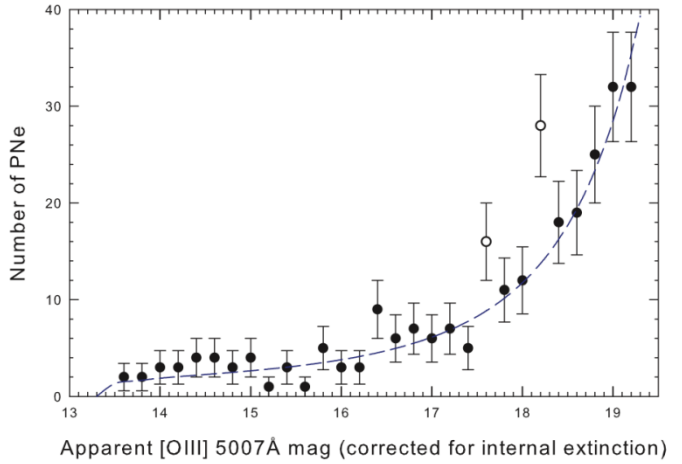

Planetary Nebula Luminosity Function

Cumulative PNLF

$$K(M) = \frac{c^1}{c^2}[e^{c_2 M} - e^{c_2 M^*}] - \frac{c_1 e^{3M^*}}{(c_2 - 3)}[e^{M(c_2-3)} - e^{M*(c_2-3)}]$$

Méndez et al. 1993

C1 = 0.307
C2 = 12 for SMC and 8 for LMC

The percentage of PNe at each luminosity bin represents the percentage of time PNe spend at that luminosity according to predictions of Jacoby (1980); Ciardullo et al. (1989) and Ciardullo et al. (2004). This plot ignores the possible incompleteness of the faint end. It is also insensitive to any intrinsic variation and `birth-to-death' luminosity range for a given PN. A simulated increase of the faintest 2 magnitudes would further decrease the percentages at the bright end.

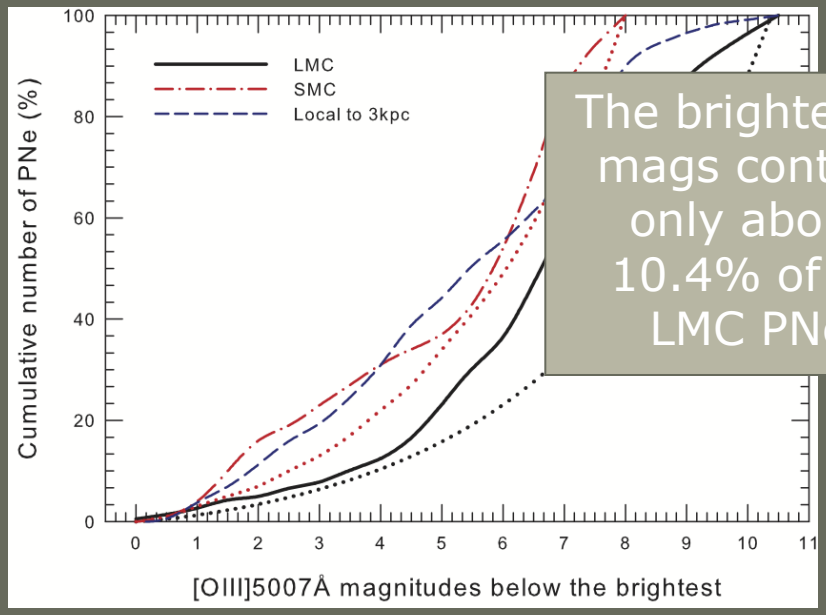

The brightest 4 mags contain only about 10.4% of all LMC PNe

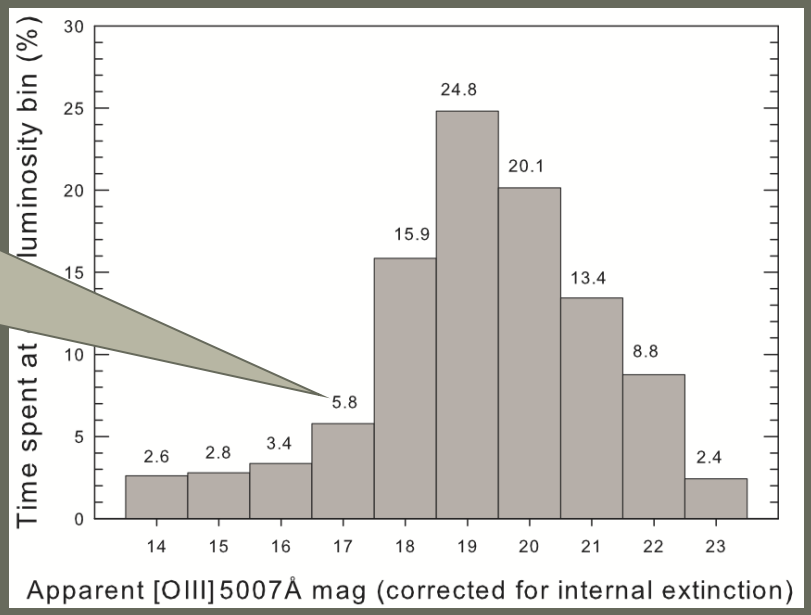

Reid & Parker 2010 MNRAS 405, 1349

Spectral Diagnostics

Dynamical age

$T_{dyn} = 890\ (M_{neb}\, V_{exp})^{0.6}\ yr$

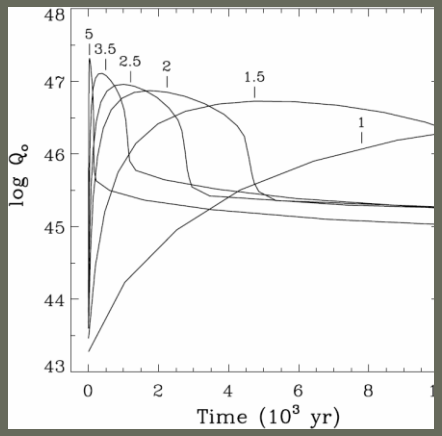

Left: The number of ionising photons Q_o is shown for the first 10,000yrs of central star evolution. Each line is marked with the initial mass model. This graph was designed by Villaver et al. (2002) using simulations, however there is a very good agreement between the model and dynamical ages derived in this work.

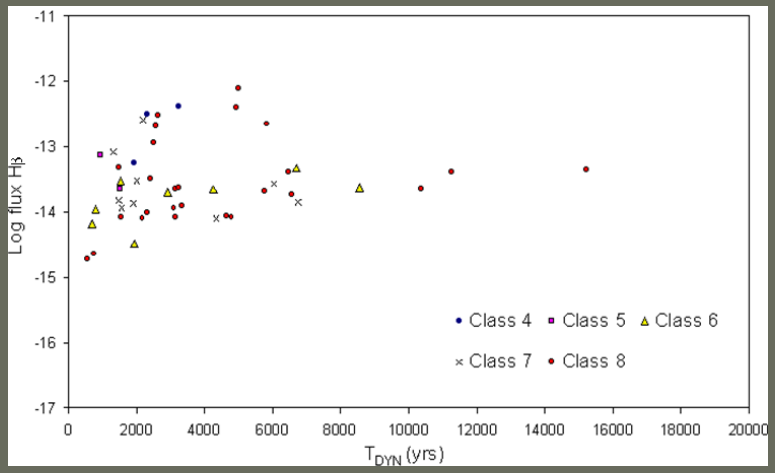

Medium excitation

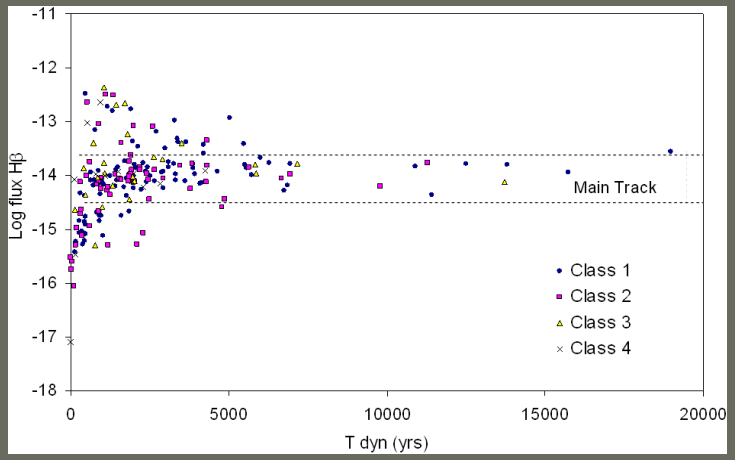

Low excitation

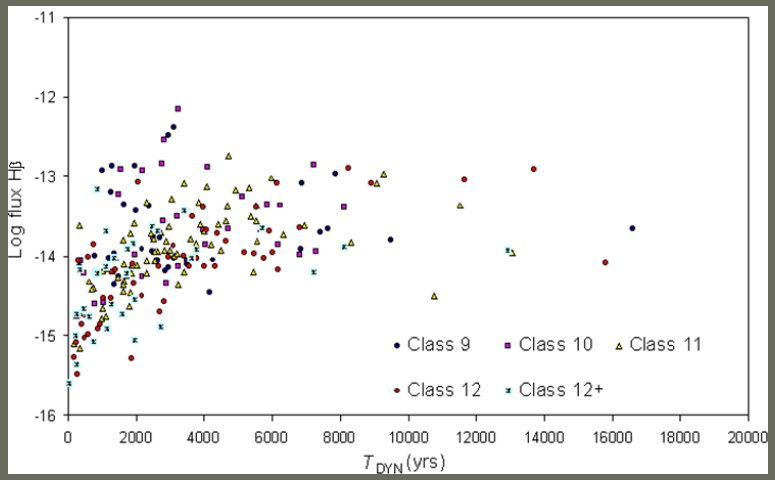

High excitation

PNLF using Hβ

Reid & Parker 2010 MNRAS 405, 1349

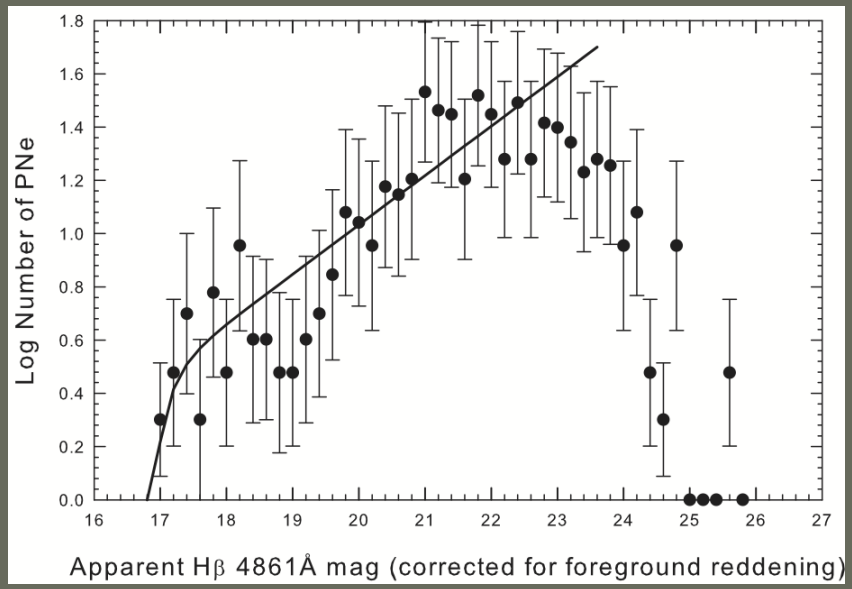

For optically thick PNe, the Hβ flux should be a reliable indicator of stellar luminosity. The conversion efficiency from stellar luminosity to Hβ luminosity is a function of stellar effective temperature and metallicity.

Peak efficiency occurs at about T_{eff} = 70,000K, broadly encompassing PNe from magnitudes 19.7 to 23.7.

The ratio [OIII]5007/Hβ largely depends on T_{eff} and metallicity.

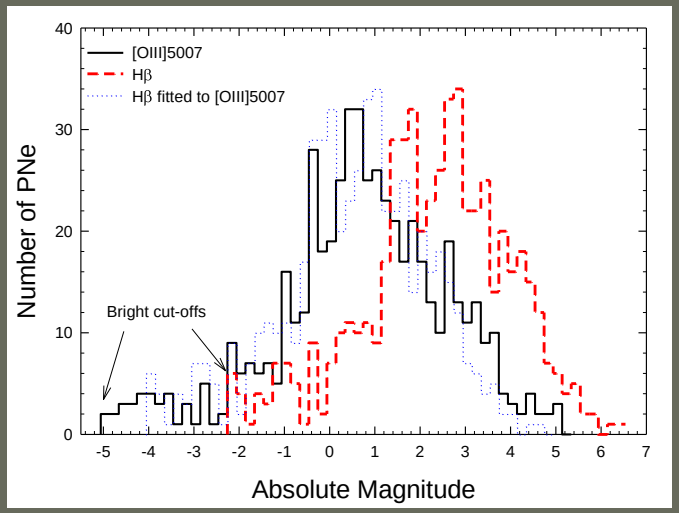

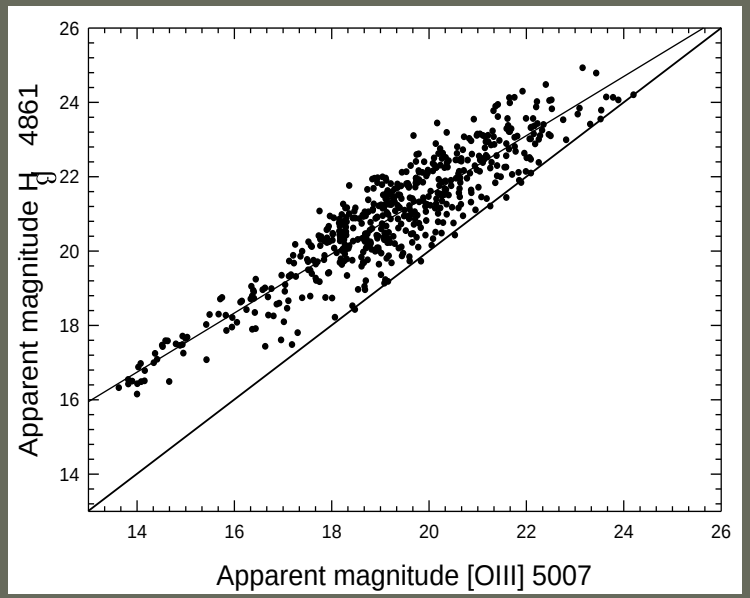

LMC PNLF in Hα

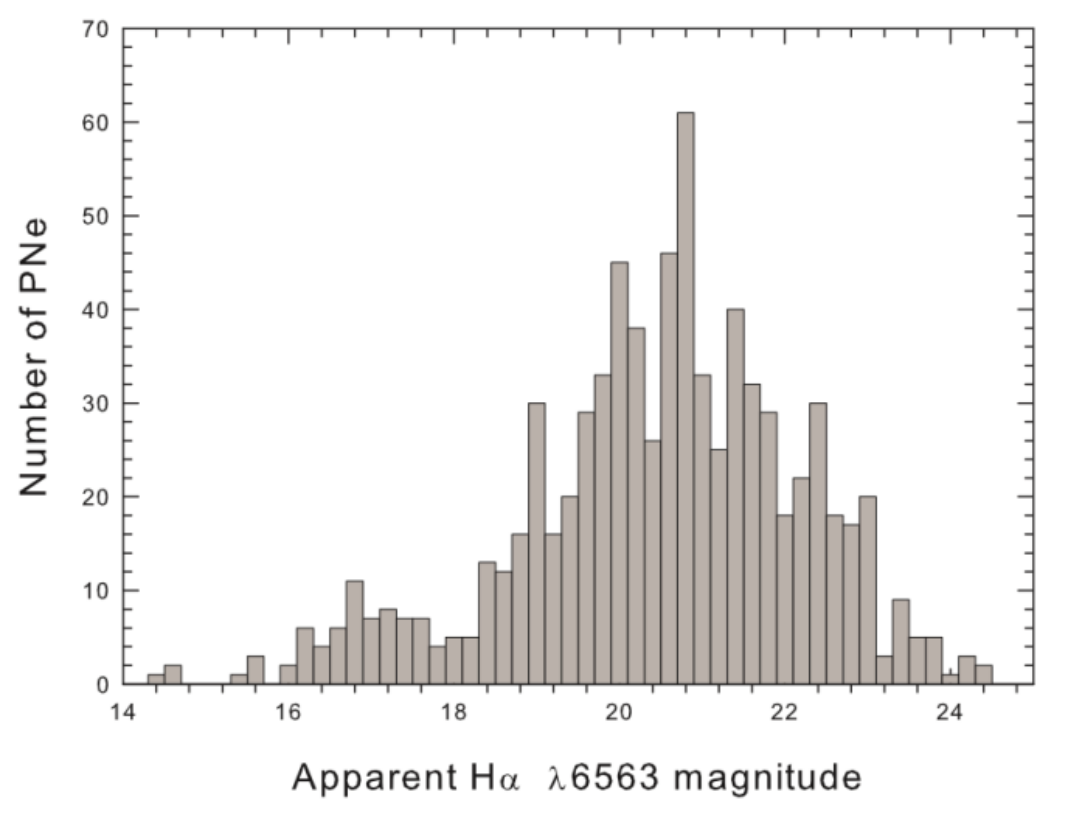

PNLF in the MIR using IRAC

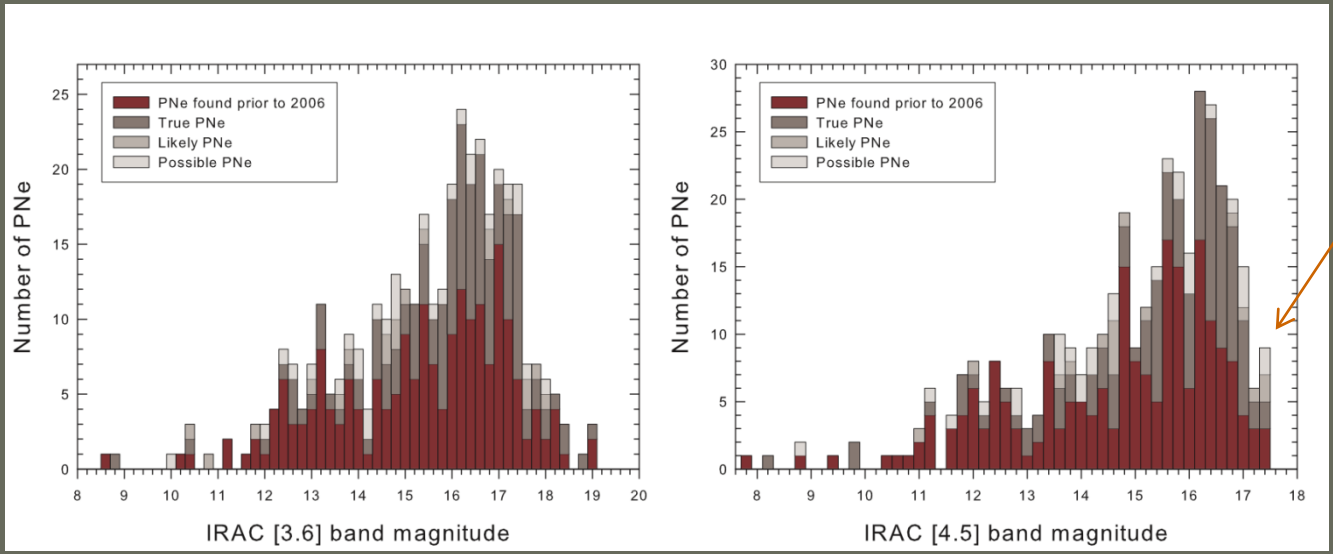

Detection limit of the Spitzer Space telescope for LMC emission objects

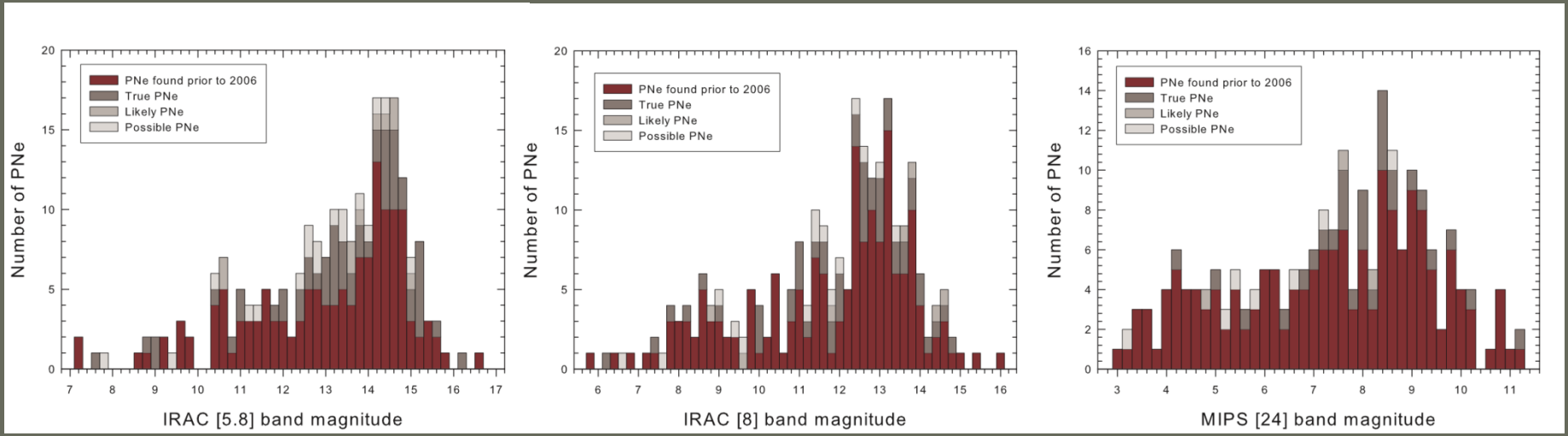

Combined PNLF using MIR [3.6], [4.5], [5.8], [8], [24] bands

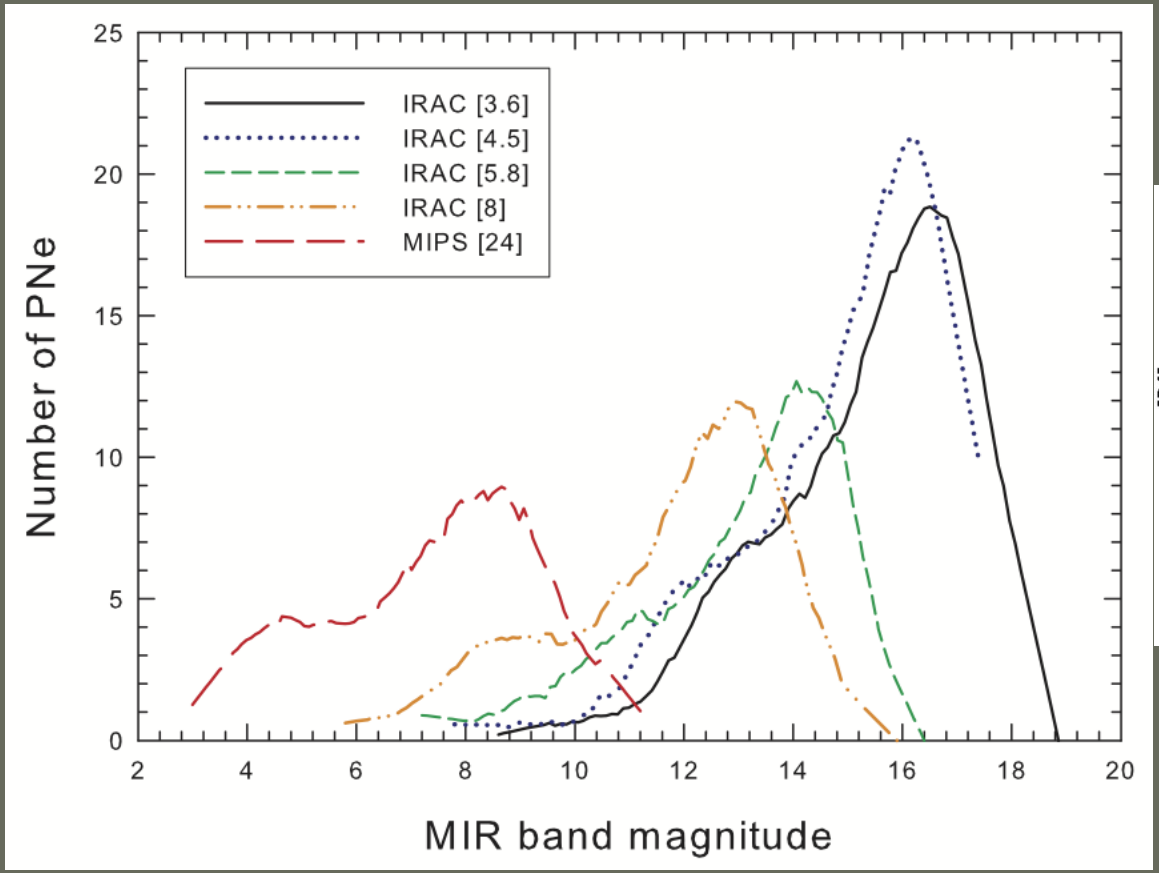

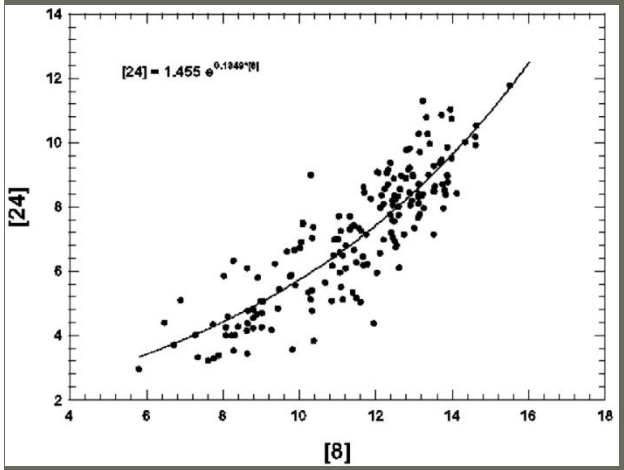

The IR Surveys

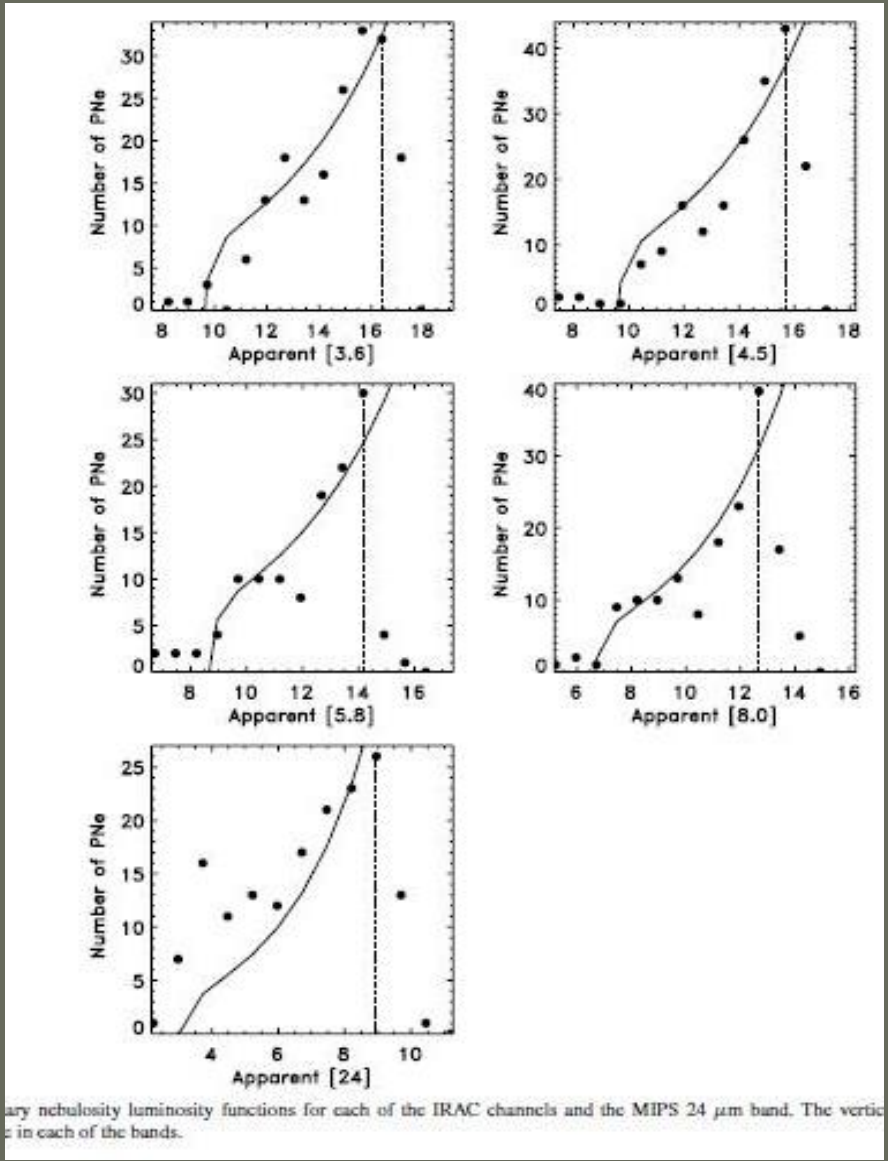

ary nebulosity luminosity functions for each of the IRAC channels and the MIPS 24 μm band. The vertic
in each of the bands.

Hora et al. 2008 ApJ., 135, 726

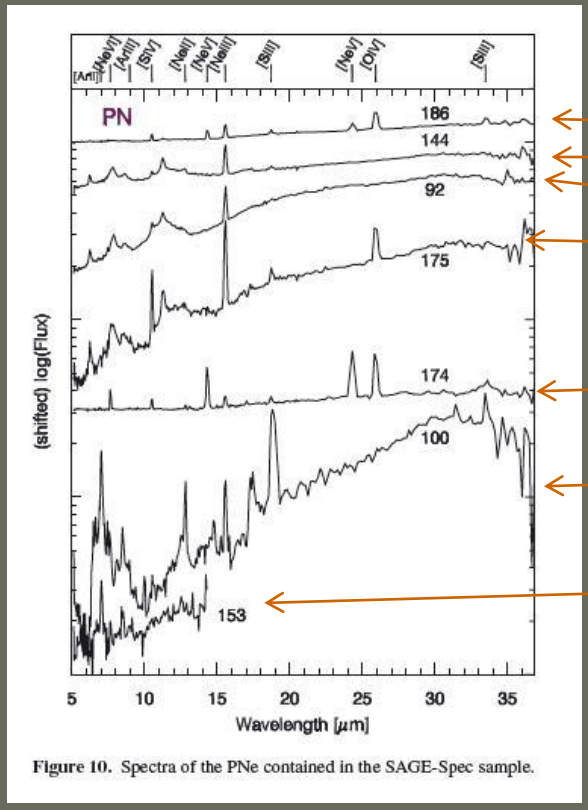

Figure 10. Spectra of the PNe contained in the SAGE-Spec sample.

N170 O-rich
N151 C-rich
N125 C-rich
N178 C-rich
LM2-42 O-rich
N136 VLE O-rich
RP493 O-rich

Woods et al. 2011 MNRAS., 411, 1597

MIR colour-colour comparison

PNe with emission-line spectra and little or no dust continuum

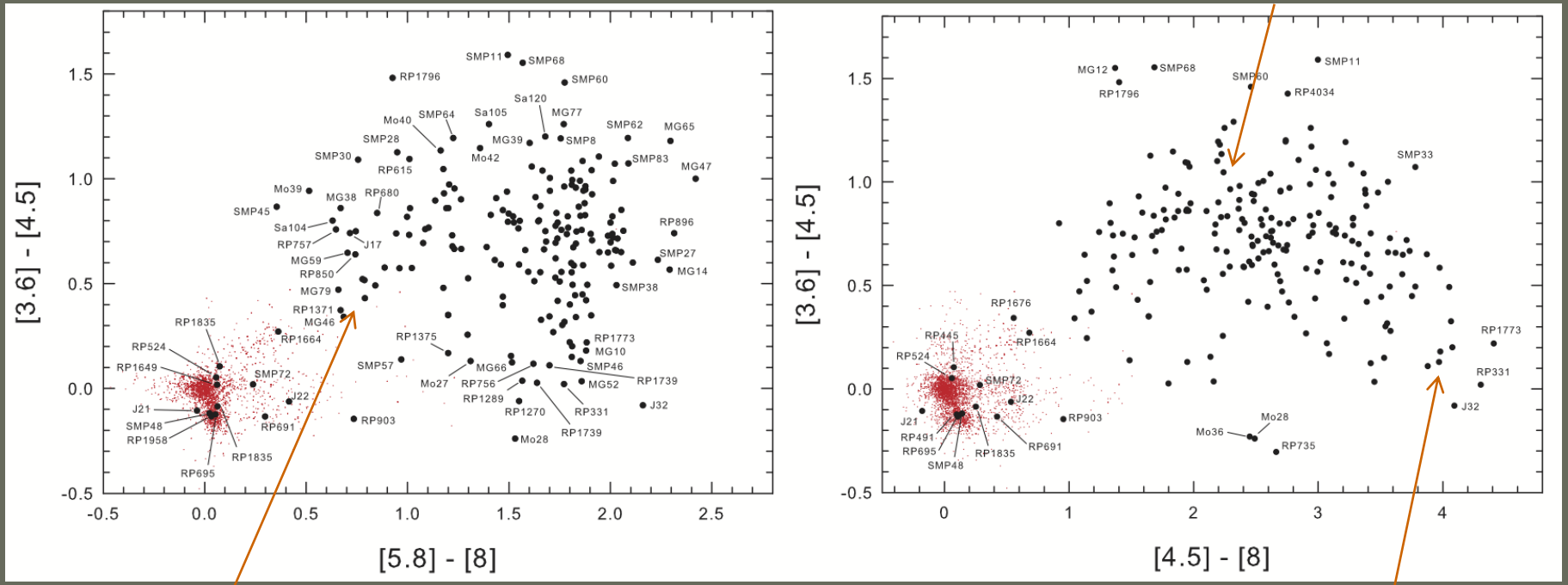

Featureless in the MIR

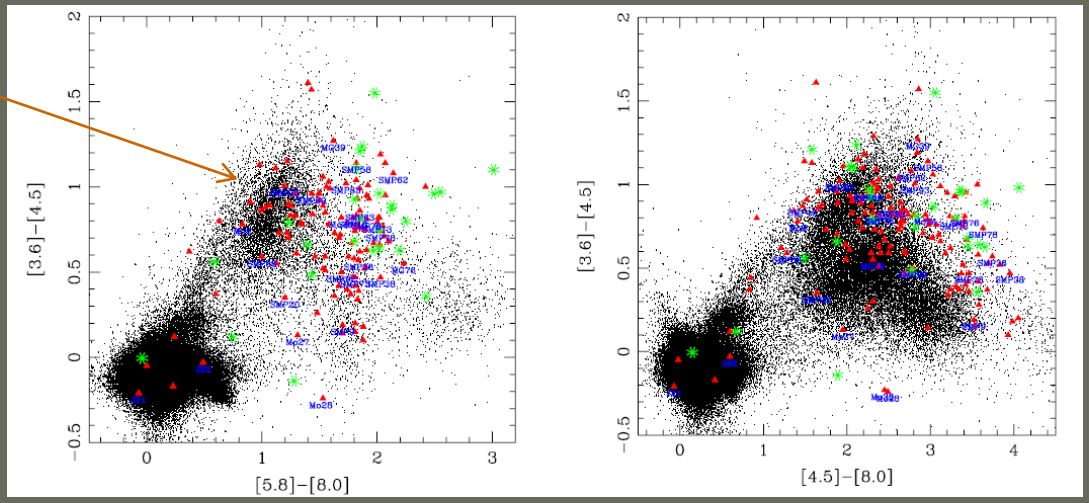

Strong continuum emission from warm dust + PAHs

NIR & MIR colour–colour comparison

Extreme AGB stars

SMP 38 and 76 appear at the red end

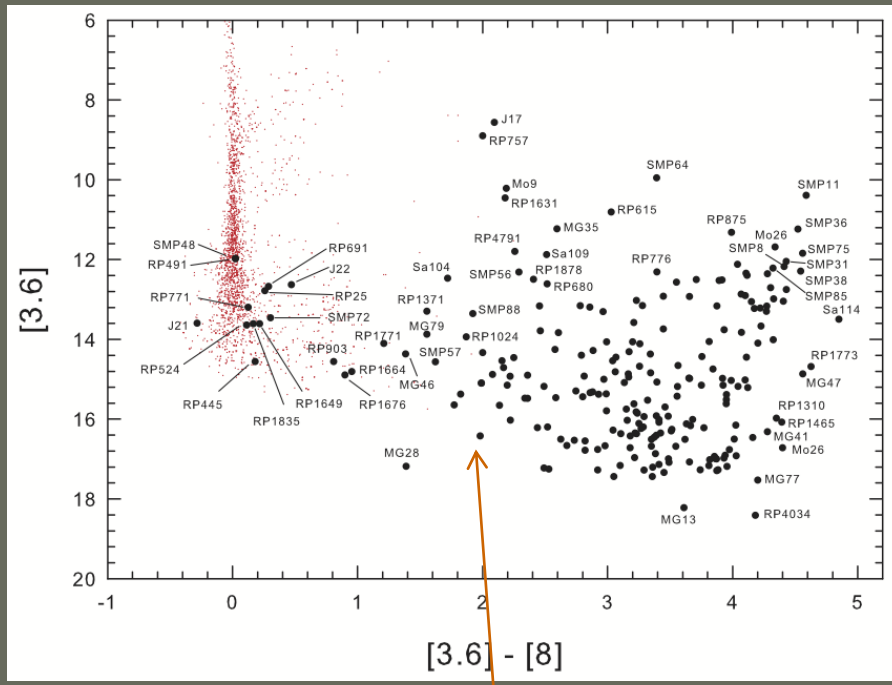

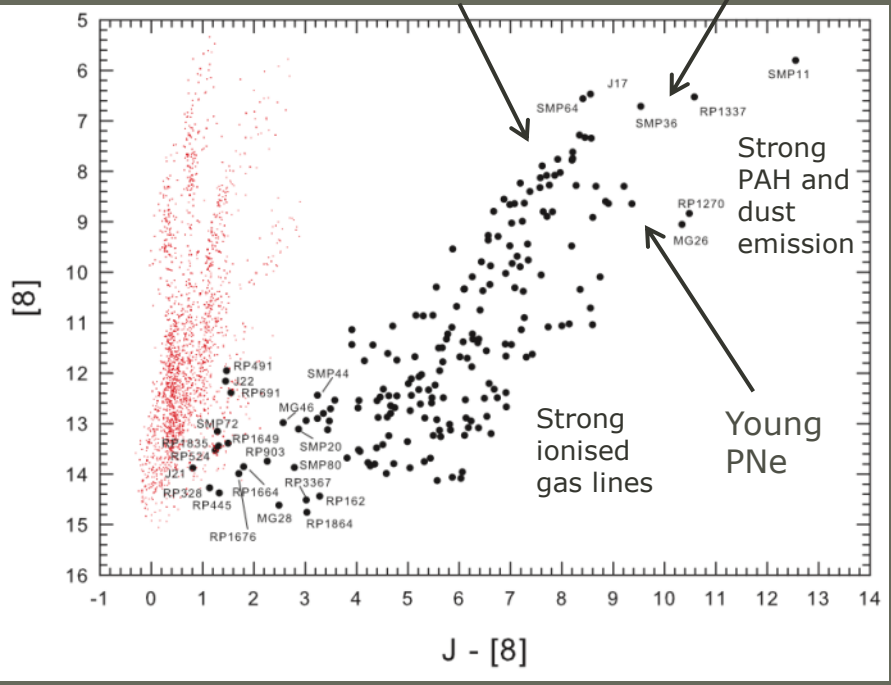

Strong PAH and dust emission

Strong ionised gas lines

Young PNe

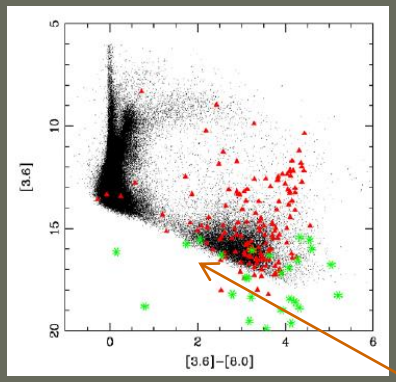

Decreasing sensitivity cut-off starlight increasingly replaced by PAH and H Pfγ emission

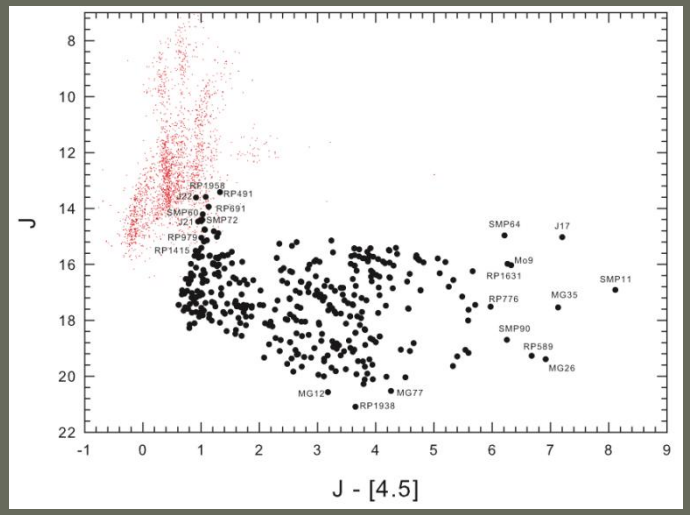

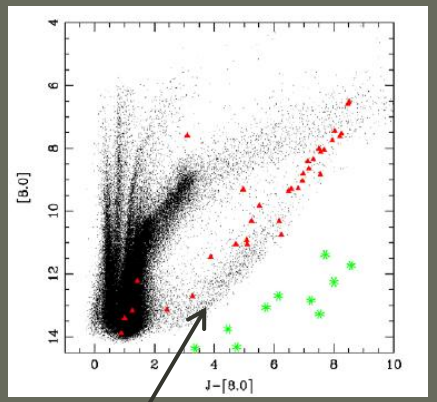

Galaxy candidate (+ YSO) distribution

NIR & MIR colour–colour comparison

These PNe contain carbon or oxygen-rich dust, probably including some combination of PAHs, Paβ nebula emission and possibly silicates.

This plot maps the stellar continuum levels and some effects on warm dust components.

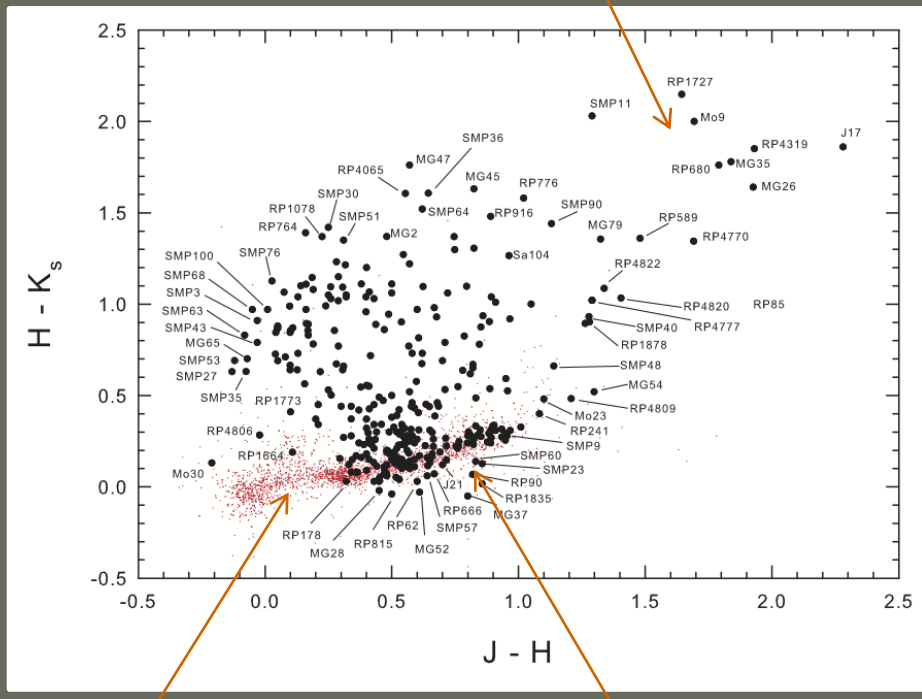

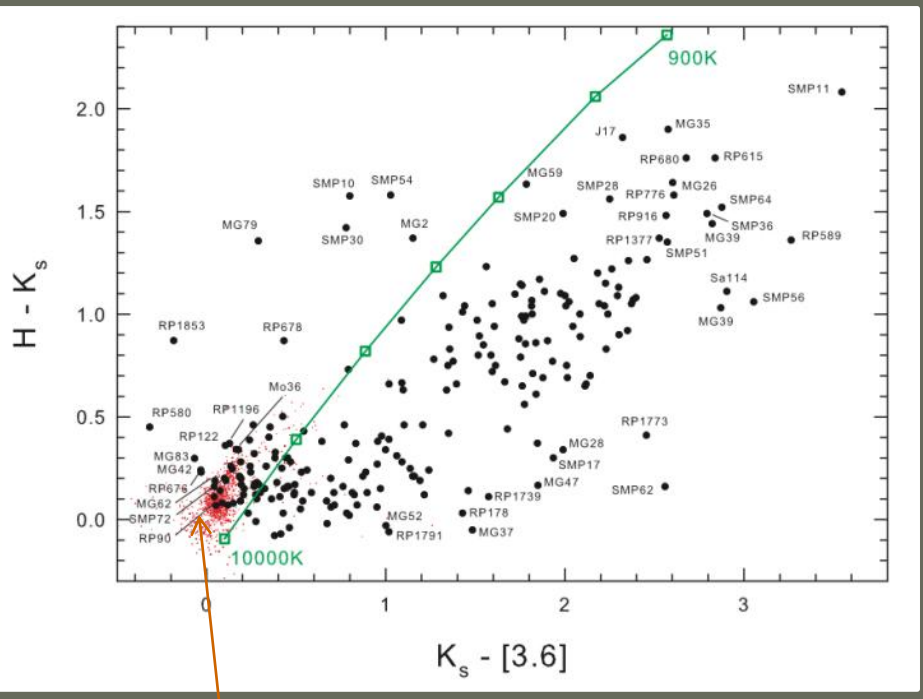

O/B stars

M Late-type stars

This separation of PNe into 2 groups, one centered on the stars and one above and more dispersed was first seen by Allen & Glass (1974).

PNe at this end of the plot have medium to low levels of 8μm emission and probably only cool dust emission

Blackbody temperatures shown are at levels of 900K, 1000K, 1250K, 1500K, 2000K, 10000K

U-B & NIR colour-colour comparison

PNe along this stellar boundary have very low dust reddening and/or have evolved to the point where the central star is unable to fully ionise the nebula. Such nebulae are ionisation-bound.

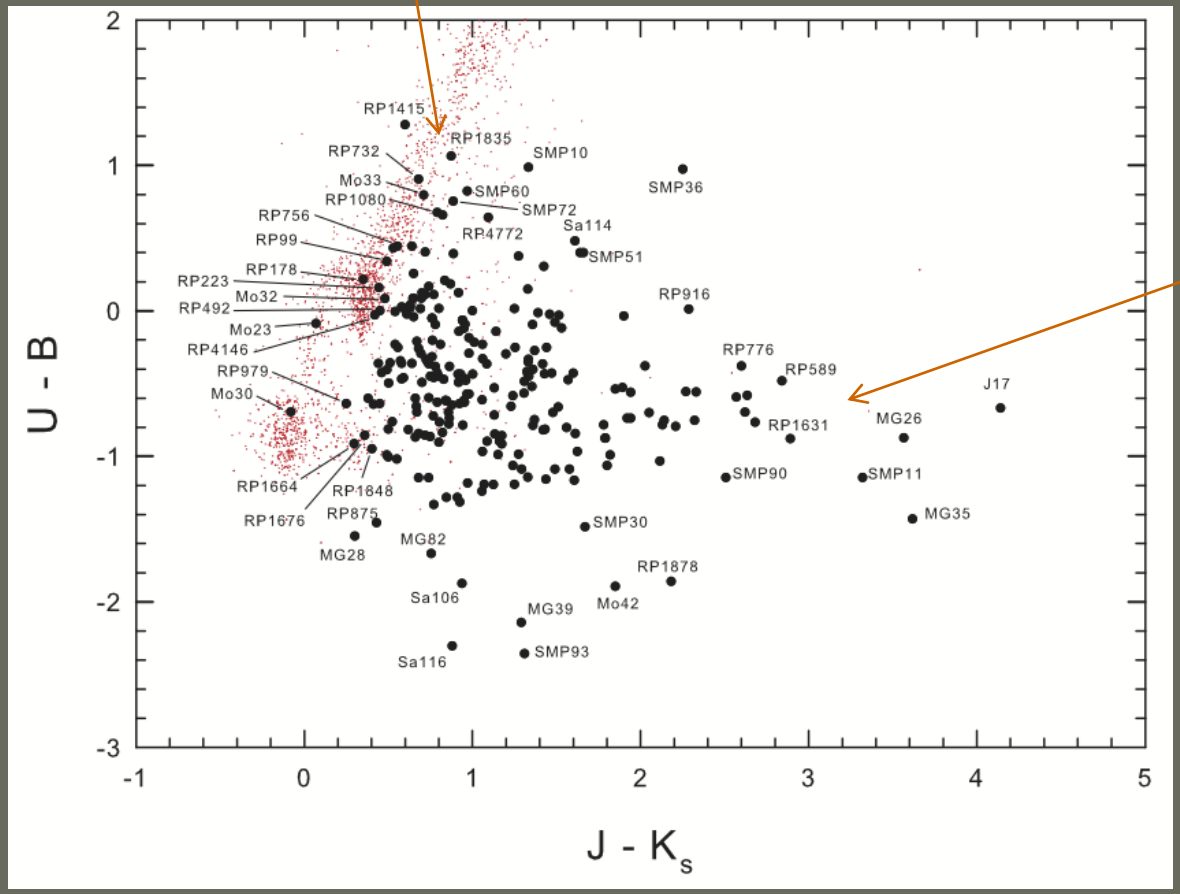

PNe with very hot dust. An area of the plot where we might expect to find symbiotic stars.

LMC PNe in the IR

Hora et al. 2008 ApJ., 135, 726

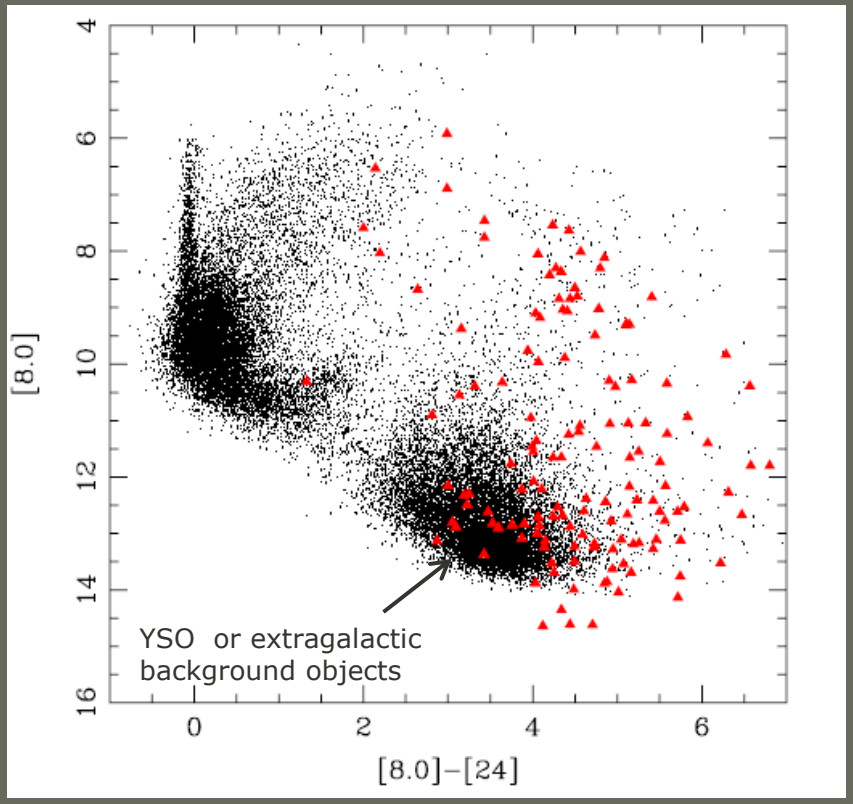

Fig. 8 [8.0] versus [8.0]-[24]

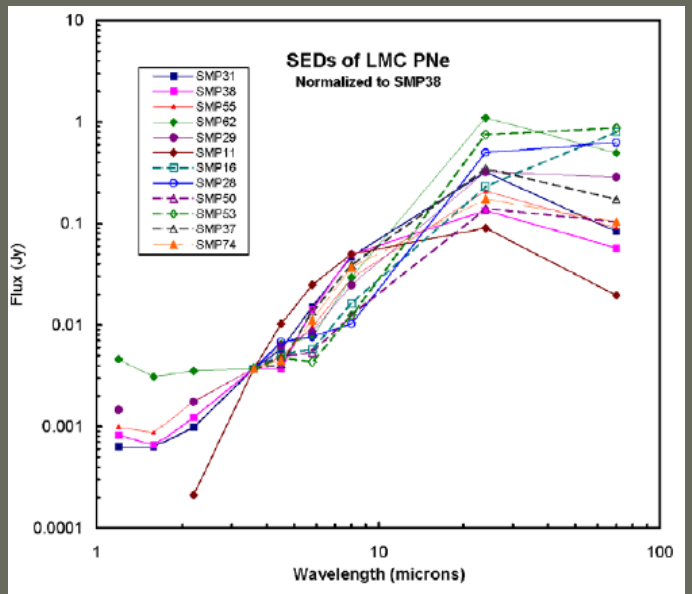

PN SEDs
1.2 – 70μm

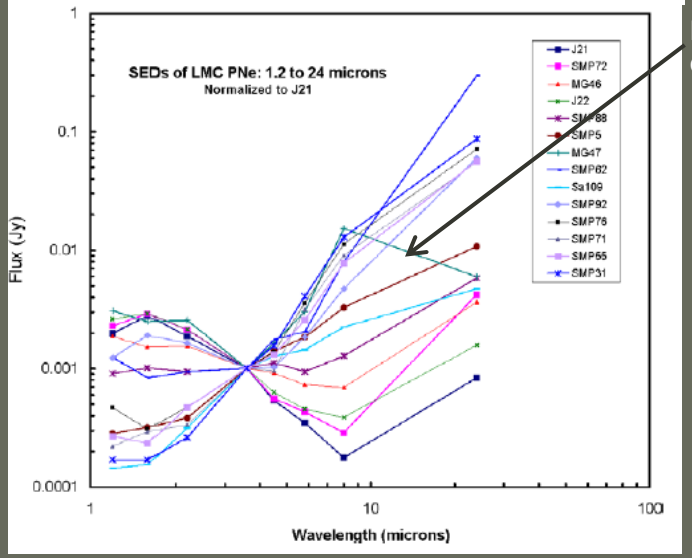

MG 24 Warm
dust component ?

PN SEDs
1.2 – 24μm

SED's for Carbon-Rich to Oxygen-Rich PNe

IR Analysis

SPITZER INFRARED SPECTROGRAPH OBSERVATIONS OF MAGELLANIC CLOUD PLANETARY NEBULAE: THE NATURE OF DUST IN LOW-METALLICITY CIRCUMSTELLAR EJECTA

25 PNe in the LMC,
16 in the SMC

Prominent silicon carbide feature at 11μm

Type F (featureless)

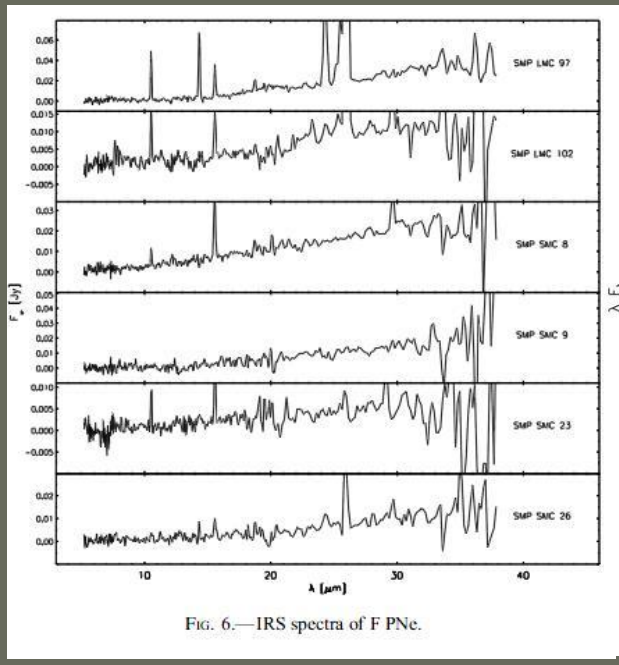

FIG. 6.—IRS spectra of F PNe.

Absence of grain emission as expected for evolved PNe

Type CRD (carbon-rich dust)

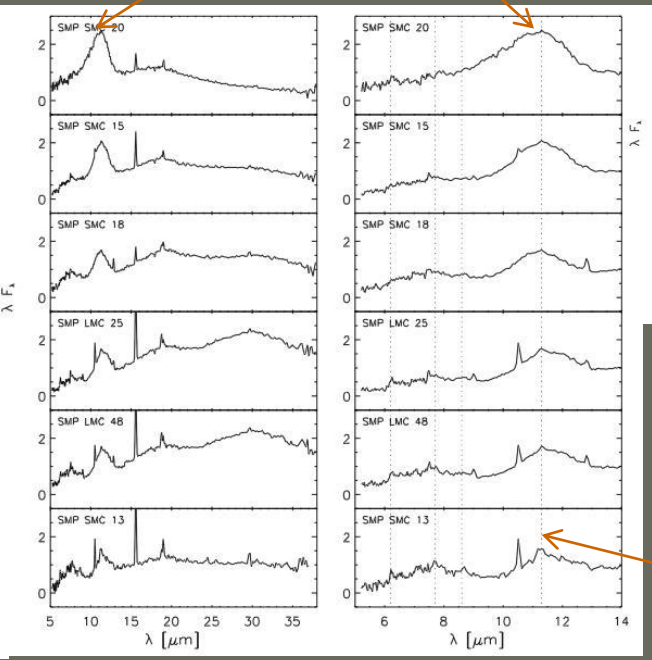

Type ORD (oxygen-rich dust)

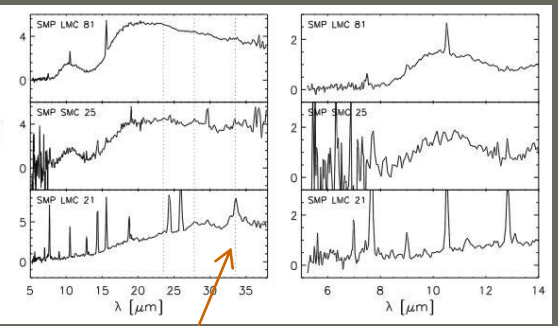

Crystalline silicate features 23.5, 27.8, 33.5mm

Classic PAH emission features at 3.3, 6.2, 7.7, 8.6 and/or 11.3μm

The low dust continuum and absence of features in LMC PNe has not been observed in Galactic PNe

Stanghellini et al. 2007 ApJ 671, 1669

△ = F
◇ = CRD
□ = ORD

IR analysis

● = round
◆ = elliptical
▲ = bipolar core
■ = bipolar, quadrupolar

IR luminosity vs. carbon abundance

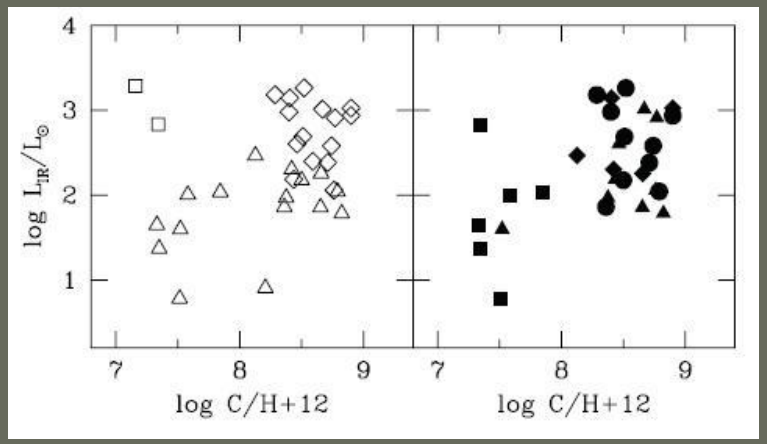

Dust temperature vs. IR luminosity

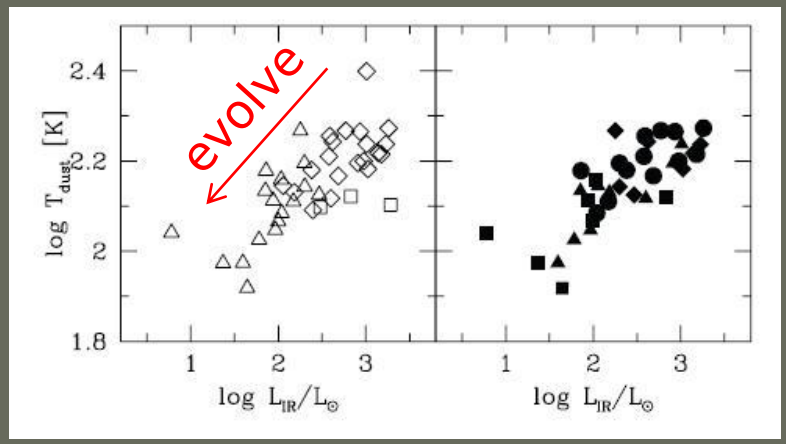

Carbon vs. oxygen abundance

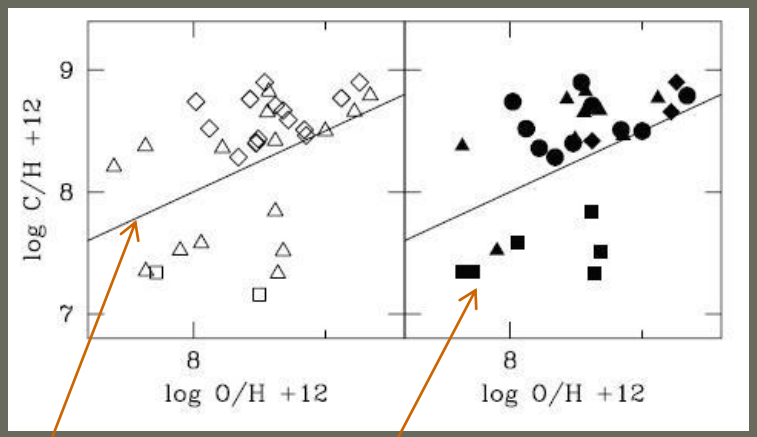

C/O = 1

Asymmetric PNe have low carbon.
O-rich dust or no dust

Dust temperature vs. Electron density

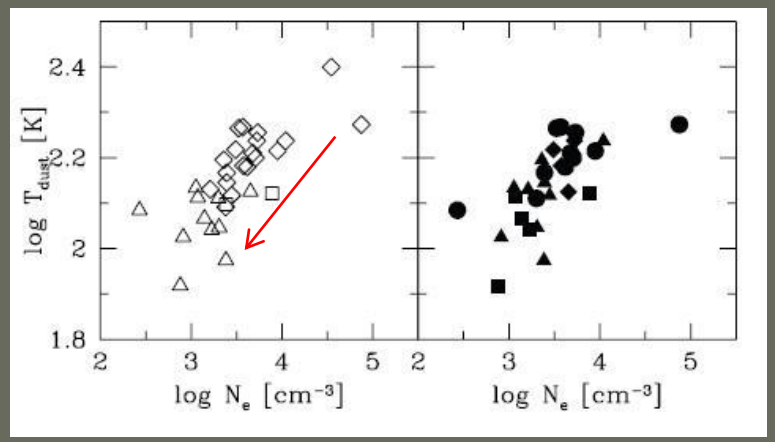

Stanghellini et al. 2007 ApJ 671, 1669

Abundances

Method

An empirical method of abundance determination, similar to that of Aller (1984) has been used. It is the system which applies ionisation correction factors (ICFs) based on grids of photoionisation models of nebulae as used by Kingsburgh & Barlow (1994). The measured intensity ratios of the lines emitted by the ions provide the abundance ratio. For example, the ratio O^{++}/H^{+} is derived by:

$$O{+}{+} / H = \frac{[OIII]\lambda 5007 / H\beta}{{}^{j}[OIII]_{(Te,ne)} / {}^{j}H\beta_{(Te)}}$$

Where ${}^{j}[OIII]_{(Te,ne)}$ is the emission coefficient of the [OIII]5007Å line which depends on T_e and n_e and ${}^{j}H\beta_{(Te)}$ is the emission coefficient of Hβ, which depends on T_e. The total oxygen abundance relative to hydrogen is then found by adding all of its ions so that:

$$O/H = O^{+} / H^{+} + O^{++} / H^{+} * ICF\ O$$

Aller L.H., 1984, Physics of Thermal Gaseous Nebulae, vol.112, Astrophysics and Space Science Library, D. Reidel Dordrecht, Holland.
Kingsburgh R.L., Barlow M.J., 1994, MNRAS 271, 257

Abundances

Type I PNe

He / H > 0.10 and $N^+/O^+ > 0.25$

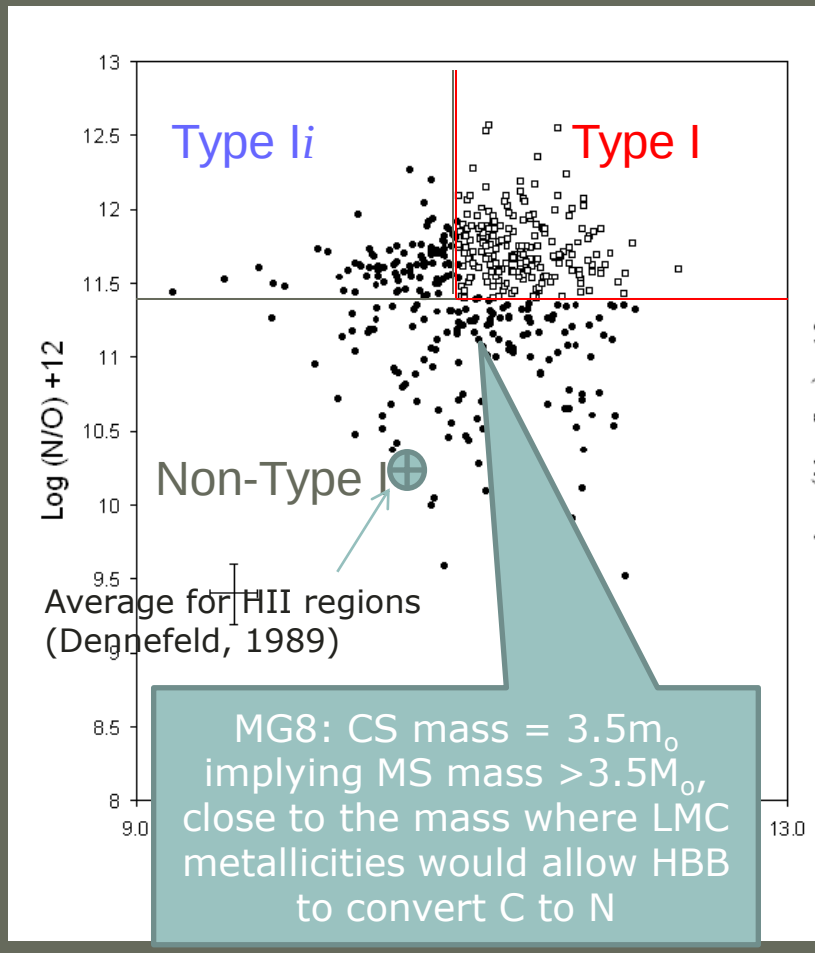

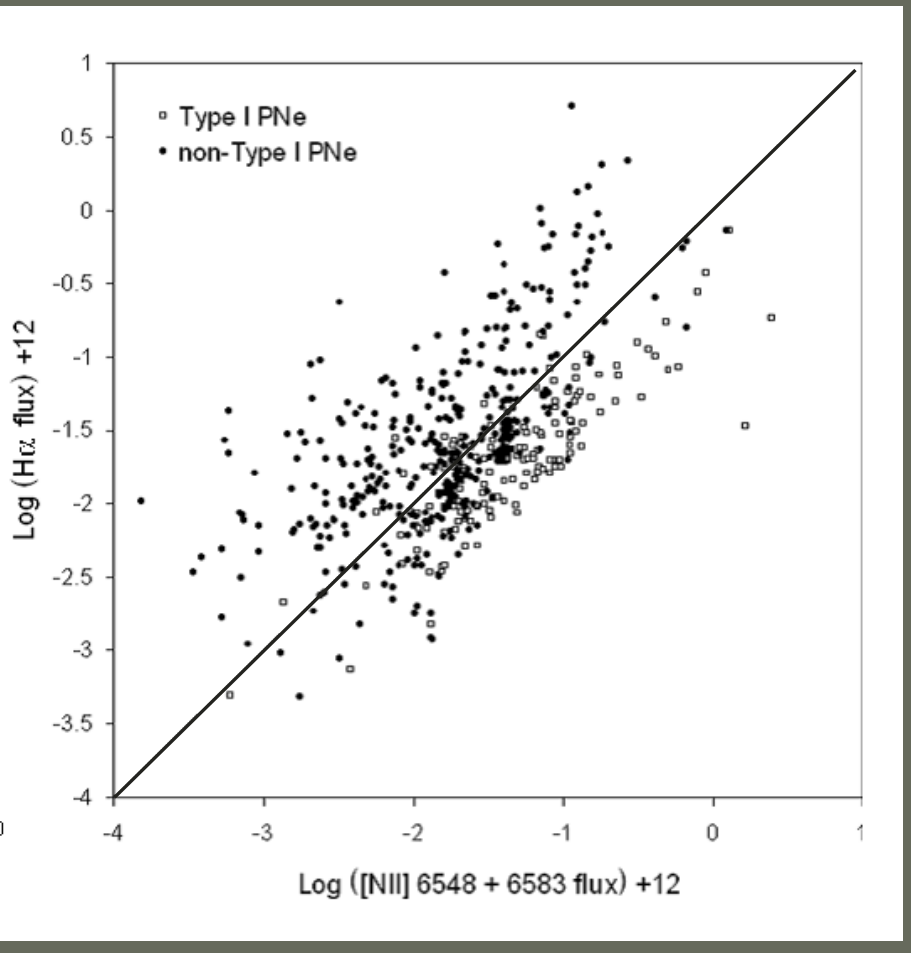

Abundances- Type I (Blue)

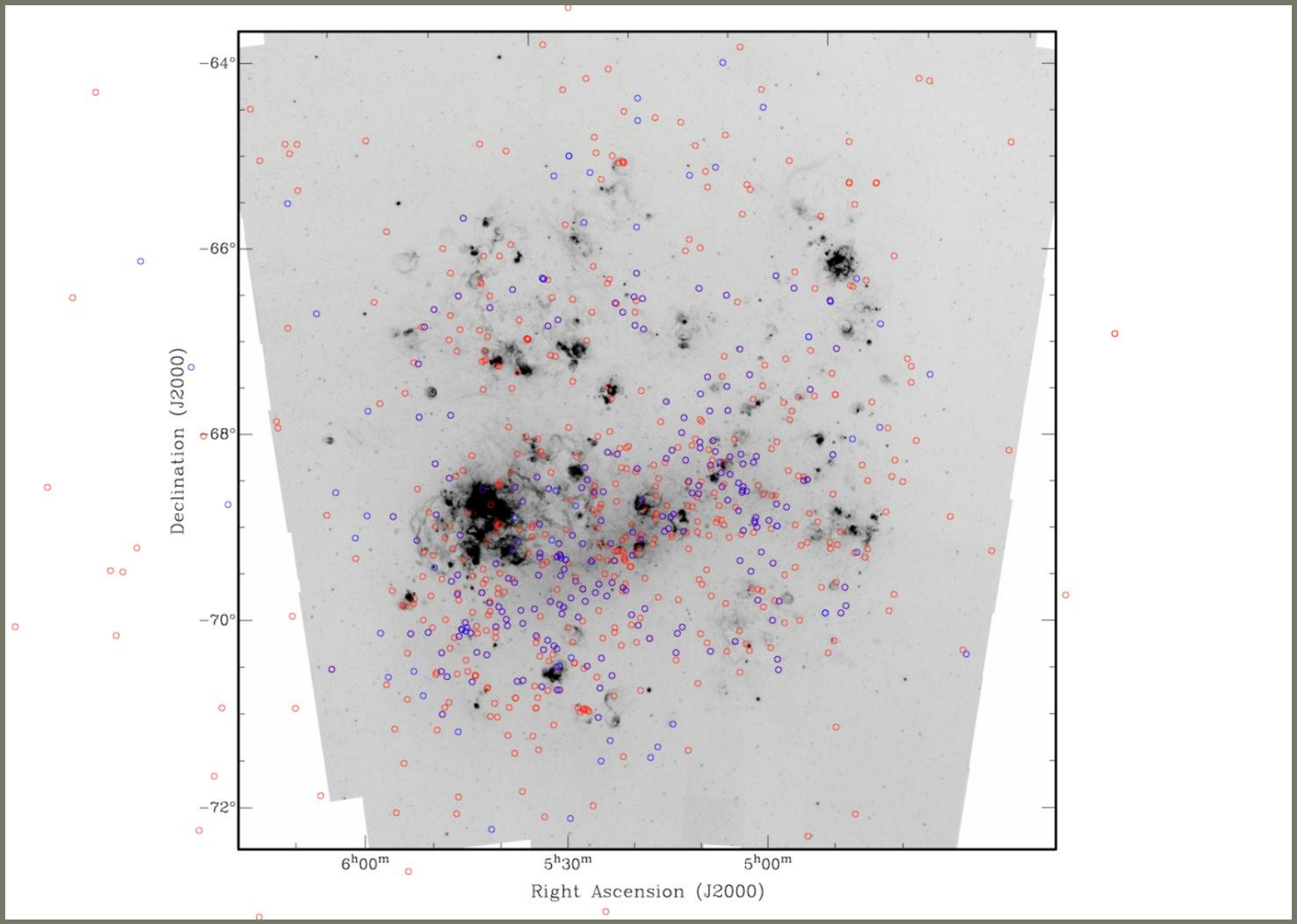

2006 MNRAS 373, 521

Radial Velocities

The need for an accurate and comprehensive LMC PN velocity study

Survey	Telescope	Res. or Disp.	λ for V_R	V_R disp (km/s)	N_{PNe}	$V_{grad\ max}$ degrees
Feast 1986	74" SAAO	49Å/mm	Hγ	22±3	25	171
Webster 1969	74" MSO	140,50Å/mm	3 R, 6 B	24±5	24	171
Smith & Weedman 1972	36" CTIO		[O III] 5007	14.7	27	171
Meatheringham et al. 1988	1-m, 2.3-m,	11.75 km/s	[O III] 5007	20	94	-
"	3.9-m AAT					
Boroson & Liebert 1989	2.5-m LCO	3.5Å/pixel	Hβ, [O III] 5007	-	24	-
Vassiliadis et al 1992	2.3-m SSO	11.5 km/s	[O III] 5007	-	16	-
Morgan & Parker 1998	1.2-m UKST	1.34Å/pixel	cross cor	-	96	-
"			4550-5500Å			
This work	3.9-m AAT	1.1Å/pixel	6200-7300Å	20.6±8	587	122

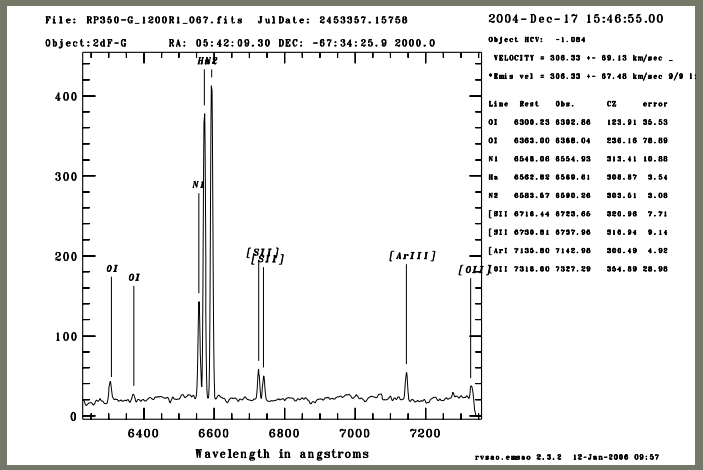

Emission line

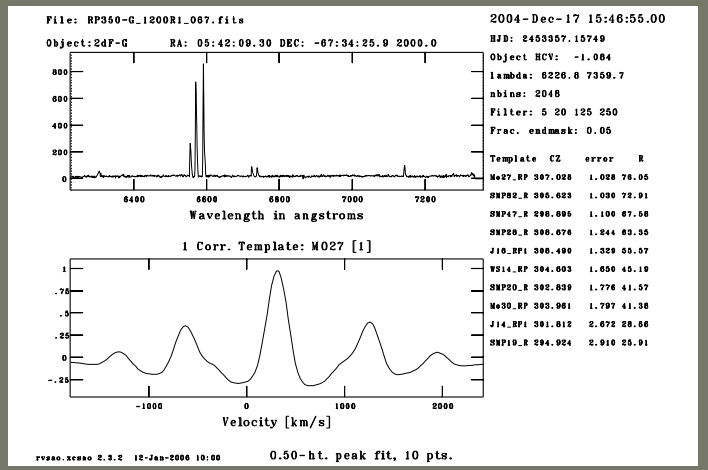

Cross-correlation

Radial Velocities

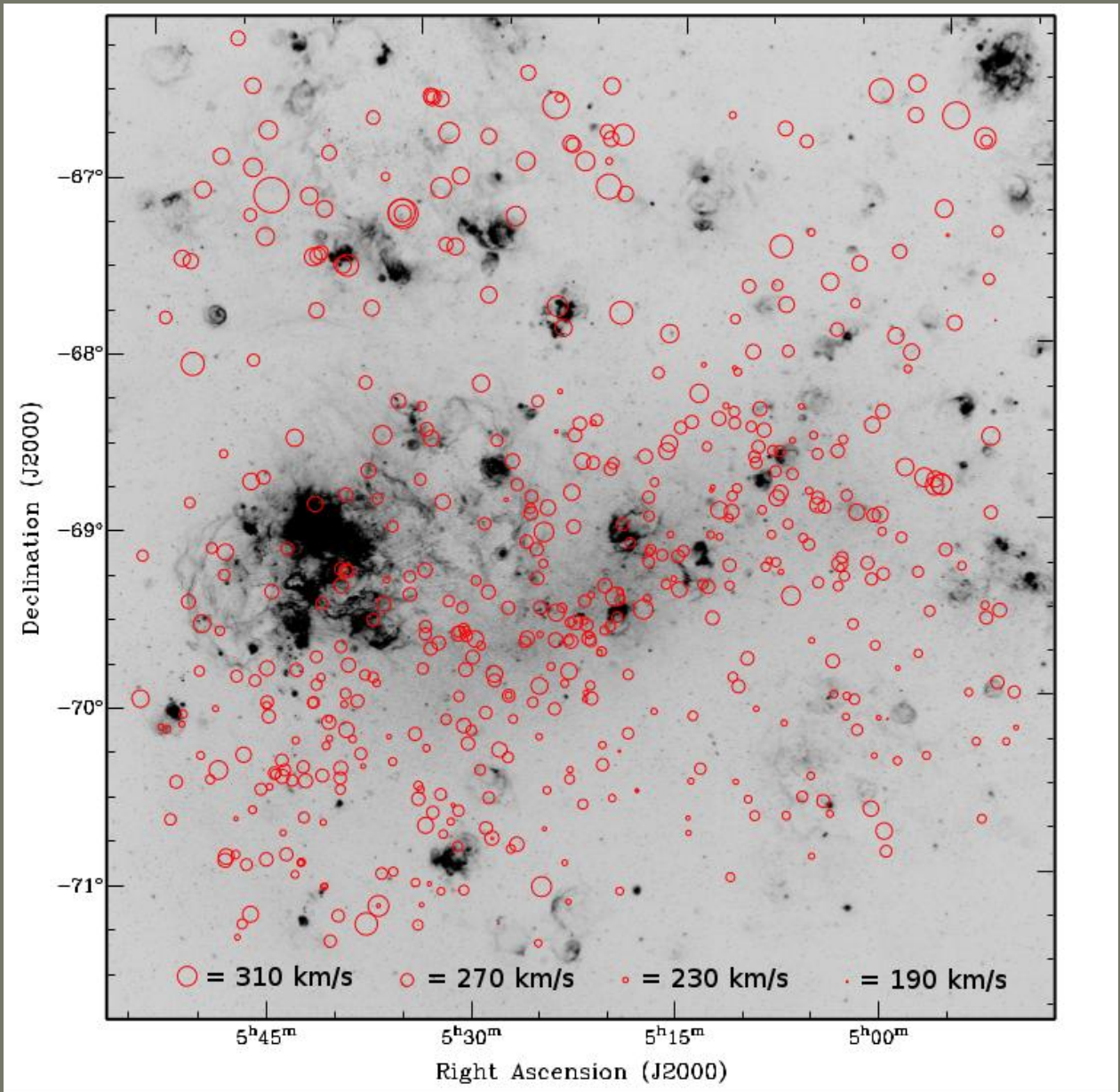

HI rotation curve

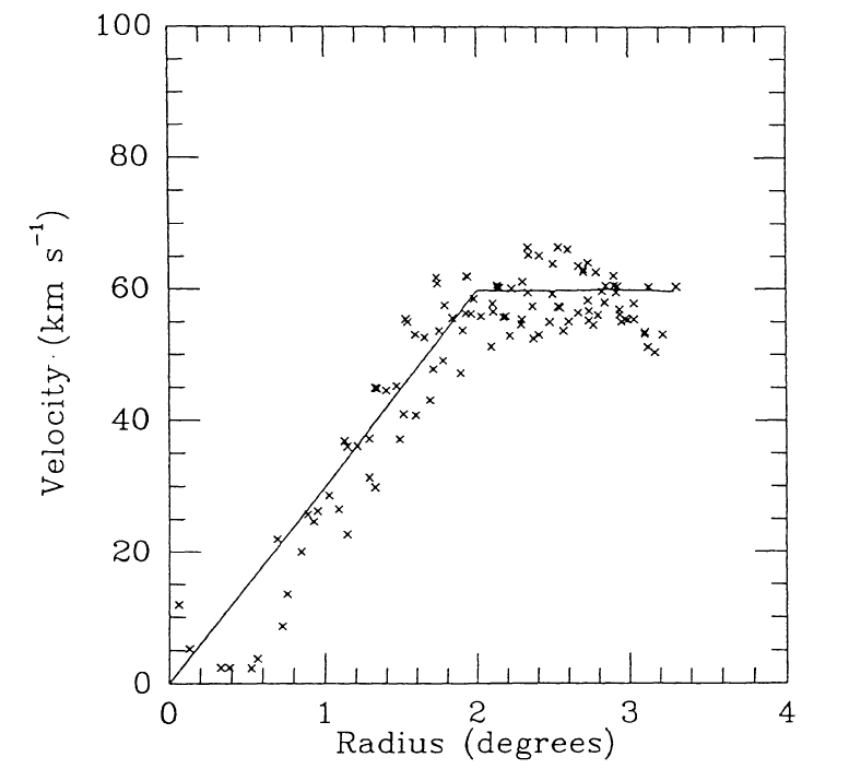

- The LMC HI rotation curve obtained after folding the HI GSR data about the central symmetrical point. The solid line represents the fitted theoretical curve comprising solid body rotation within the inner 1.5° together with an exponential and somewhat warped disk outside.

- The velocities of the HI and PNe may be de-projected from the LMC's 35° angle of inclination but the position angle for the line of nodes for each population must be derived separately. Assuming that the mean rotation velocity of the PN system is at an independent distance from the HI centre of rotation, the rotation solution may be fitted by minimising residuals in the velocity data:

$$V(\theta,r)=V_m(r)\{1\pm[\tan(\theta-\theta_0)\sec i]^2\}^{-0.5}+V_0\ (0\leq\theta\leq2\pi)$$

$V(\theta,r)$ = rotational velocity projected onto the line of sight at position angle θ and radial coordinate r. V_0 = Galacto-centric velocity of the LMC. $V_m(r)$ = derived HI rotation curve.

Meatheringham 1991

Transverse velocity and angle of inclination

LMC is a rotating flat disk however it's apparent transverse velocity of ~300kms^{-1} means that there will be a substantial velocity gradient in the direction of motion. This gradient will combine with the rotation curve to twist the lines of constant velocity.

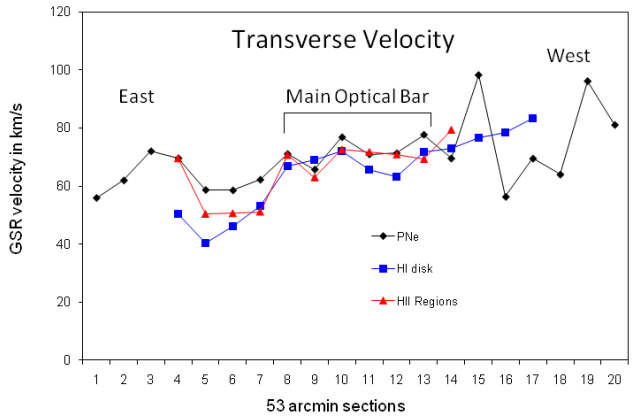

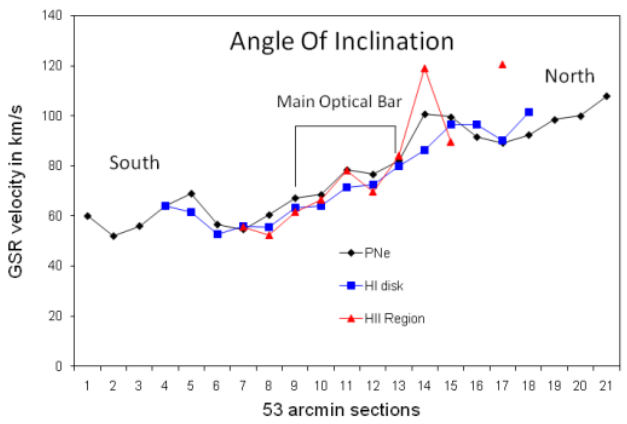

Positions are de-projected from their 35^{o} angle. The central 1.5^{o} is solid body motion and could be thought of a perturbed when compared to the HI disk to either side. This slight asymmetric positioning of the main bar may be due to gas streaming motions (Feitzinger 1983).

2006 MNRAS 373, 521

PN Kinematics within the LMC

Rotation curves for PNe and HI

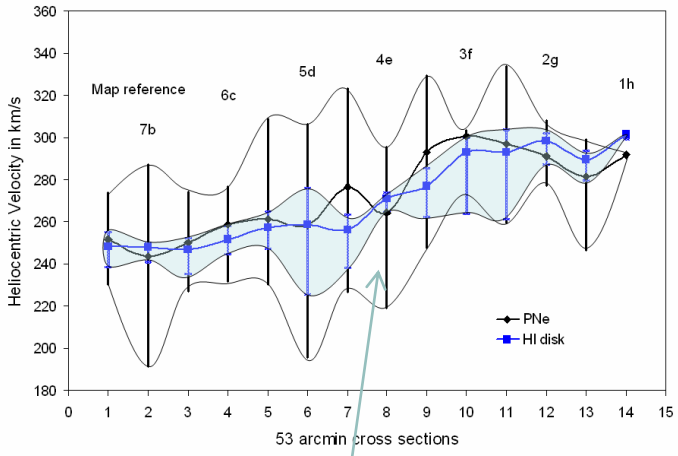

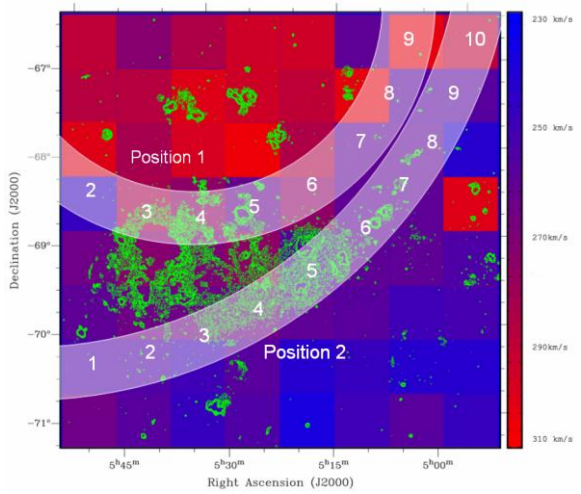

Comparison of the HI disk (blue) and PN population

The velocity dispersion is an average 3.5x higher for PNe than for HI.

Local regions of large HI velocity dispersion closely correspond to supergiant shells of star-forming activity.

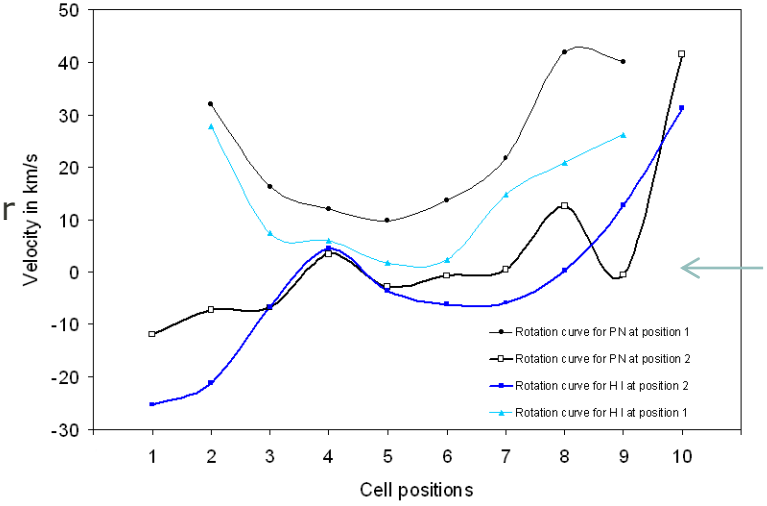

Galactocentric velocity for PNe
V_o = 42km s^{-1}

For HI disk
V_o = 46 km s^{-1}

Line of nodes
Θ_o = 170°

Summary

Parameter	Previous results	New results
Number of PNe in the central 25 deg^2 region of the LMC	164	623
Estimated number of PNe in the entire LMC	~1,000	956±141
PN magnitude range ([O III]5007Å)	6	10
Range in $c\,H\beta$ for LMC PNe	0.00 - 1.3	0.01 - 3.4
Peak in $c\,H\beta$ distribution	0.3	0.6
Range in [O III] electron temperatures t_e	> 10,600 K	7,728 - 30,107 K 80% under 20,000K
Range in [N II] electron temperatures t_e	> 7,800 K	6,646 - 30,199 K 90% under 20,000K
Range in electron densities n_e	log (2 - 4.56) g cm^{-3}	log (1 - 4.8) cm^{-3}
Peak in n_e distribution	log 3.6 cm^{-3}	log 2.2 cm^{-3}
Range in Mass$_{neb}$	0.02 - 0.94 M$_\odot$	0.01 - 0.97 M$_\odot$
Peak in Mass$_{neb}$ distribution	0.09	0.2 M$_\odot$
Number of low excitation PNe Number of medium excitation PNe Number of high excitation PNe	45 (27%) 36 (23%) 81 (50%)	247 (43%) 63 (11%) 261 (46%)
Range in derived V$_{exp}$	5.1 - 82 km s^{-1}	9.7 - 82 km s^{-1}
Mean Oxygen abundance (log +12) Mean Nitrogen abundance (log +12) Mean neon abundance (log +12) Mean sulphur abundance (log +12) Mean argon abundance (log +12)	8.1 - 8.49* 7.23 - 8.26* 7.39 - 7.80* 6.67 - 6.92* 5.88 - 6.00*	8.10 ±0.49 7.67 ±0.60 7.32 ±0.87 6.29 ±0.66 5.83 ±0.67
No. of Type I PNe in survey region	67	183
ISM nitrogen enhancement in the LMC due to PNe	6.8 × 10^{-7} M$_\odot$ yr^{-1}	2.02 × 10^{-6} M$_\odot$ yr^{-1}
Bright turnoff magnitude (M*) Distance to LMC using PNLF	-4.1 48.7 kpc	-4.1 48.7 kpc
Peak of PNLF distribution	unknown	0.6 Mag (absolute)
No. LMC PNe Vel$_{rad}$ measurements	97	587
Mean PN vertical velocity dispersion Mean HI vertical velocity dispersion	19.1 km s^{-1} 5.4 km s^{-1}	40.1 km s^{-1} 18 km s^{-1}
PN centroid (J2000) Vel$_{GSR}$ at PN centroid	$05^h23^m23^s$ -68°58^m unknown	$05^h19^m12^s$ -69°26^{m}17^s 70.7 km s^{-1}

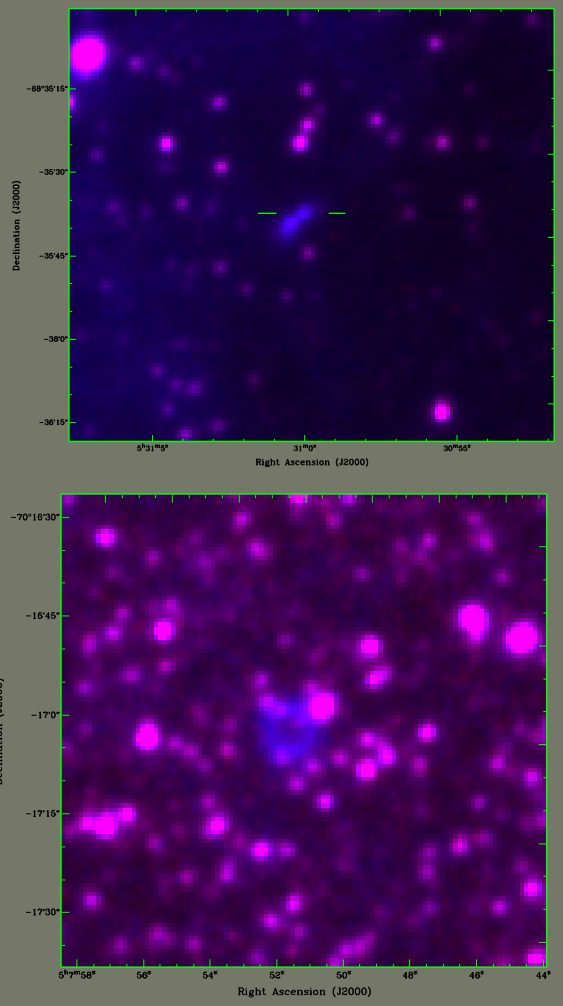

Reid, W. A., & Parker, Q. A. 2006, MNRAS, 365, 401

Reid, W. A., & Parker, Q. A. 2006, MNRAS, 373, 521

Reid, W.A., & Parker, Q.A., 2010, MNRAS, 405, 1349

Flux calibration of 2dF, 6dF and FLAMES spectra

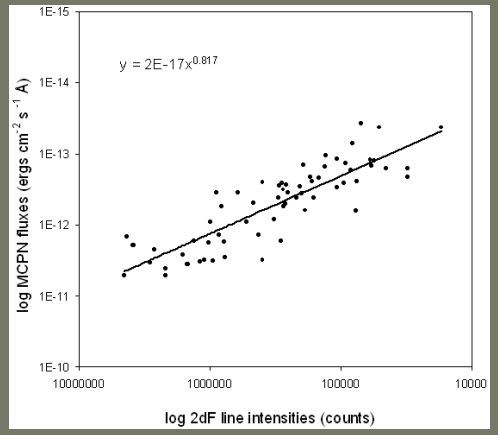

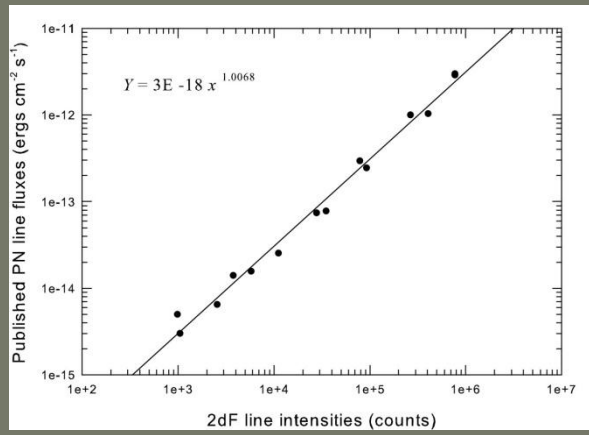

Field C ccd1

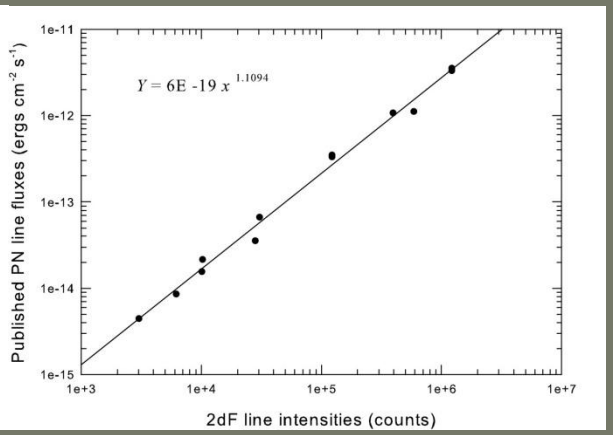

Field C ccd2

1. Raw fluxes for [OIII]5007 from MCPN are compared with 2dF line intensities for the same objects prior to calibration, regardless of ccd and field plate used.

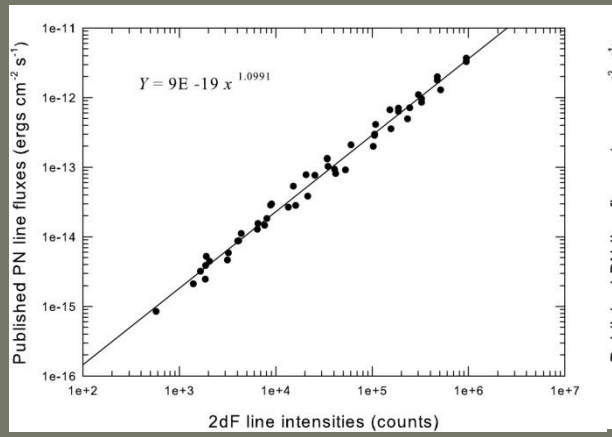

Field H ccd1

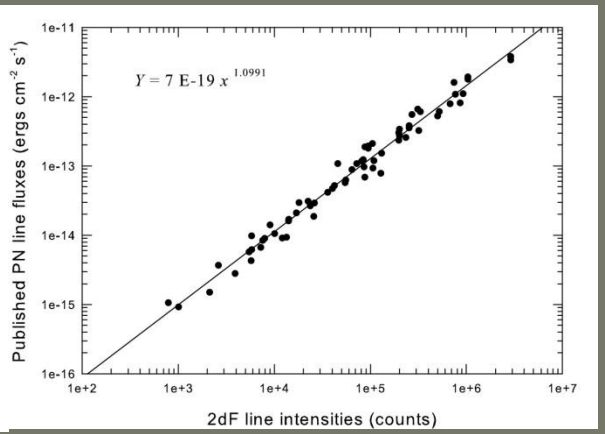

Field H ccd2

2. 2dF line intensities are matched to MCPN-based Hβ and [OIII]5007 fluxes for each ccd and field plate combination producing a equation for flux calibration.

Flux calibration of 2dF and FLAMES spectra

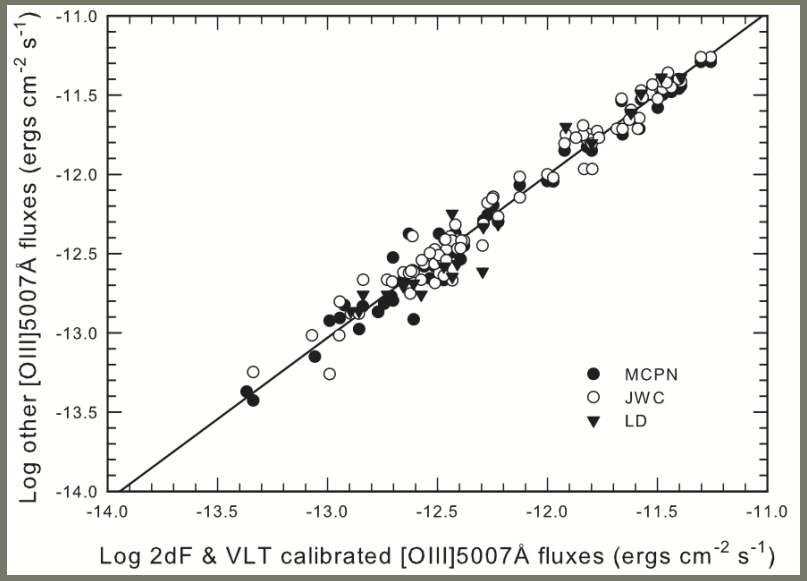

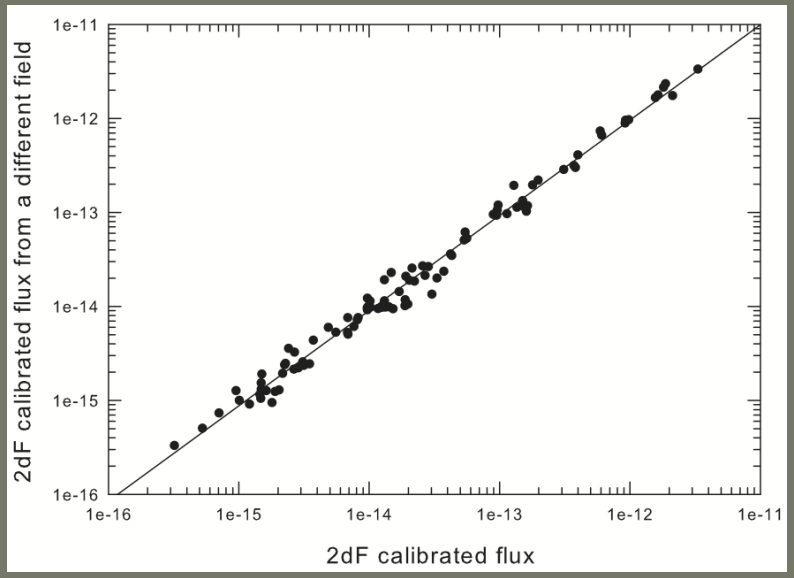

3. The calibrated [OIII]5007 2df and VLT line fluxes are plotted against fluxes for the same objects from 3 different published catalogues.
MCPN http://archive.stsci.edu/hst/mcpn/
JWC (Jacoby, Walker, Ciardullo, 1990, ApJ. 365, 471);
LD (Leisy, Dennfeld, 2006, A&A 456, 451L)

The mean agreement (RP-MCPN) is 0.03 0.10 dex. A similar mean agreement is found between RP-JWC (-0.004 0.11) and RP-LD (0.02 0.13).

The [OIII]5007 calibrated fluxes for 76 PNe with multiple observations, due to overlapping fields, are plotted in order to check the integrity of the calibration across different observations. A good match (~0.2 dex) along the line of equality has been found, where there is a mixture of fields and flux intensities represented.